fw 6110.1

REPORT NO. FRA-OR&D-75-83

DESCRIBING FUNCTION TECHNIQUES FOR THE NON-LINEAR ANALYSIS OF THE DYNAMICS OF A RAIL VEHICLE WHEELSET

Devendra P. Garg

JULY 1975
INTERIM REPORT

DOCUMENT IS AVAILABLE TO THE PUBLIC THROUGH THE NATIONAL TECHNICAL INFORMATION SERVICE, SPRINGFIELD, VIRGINIA 22161

Prepared for
U.S. DEPARTMENT OF TRANSPORTATION
FEDERAL RAILROAD ADMINISTRATION
Office of Research and Development
Washington DC 20590

03 - Rail Vehicles & Components

TECHNICAL REPORT STANDARD TITLE PAGE

1. Report No.	2. Government Accession No.	3. Recipient's Catalog No.
FRA-OR&D-75-83		

4. Title and Subtitle	5. Report Date
DESCRIBING FUNCTION TECHNIQUES FOR THE NON-LINEAR ANALYSIS OF THE DYNAMICS OF A RAIL VEHICLE WHEELSET	July 1975
	6. Performing Organization Code
7. Author(s)	8. Performing Organization Report No.
Devendra P. Garg	DOT-TSC-FRA-75-6
9. Performing Organization Name and Address	10. Work Unit No.
U.S. Department of Transportation Transportation Systems Center Kendall Square Cambridge MA 02142	RR515/R5301
	11. Contract or Grant No.
	13. Type of Report and Period Covered
12. Sponsoring Agency Name and Address	Interim Report July 1974-February 1975
U.S. Department of Transportation Federal Railroad Administration Office of Research and Development Washington DC 20590	14. Sponsoring Agency Code

15. Supplementary Notes

16. Abstract

The describing function method of analysis is applied to investigate the influence of parametric variations on wheelset critical velocity. In addition, the relationship between the amplitude of sustained lateral oscillations and critical speed is derived. The non-linearities in the model include the difference in rolling radii as a function of lateral displacement of the wheelset from its mean position, profile conicity, and gravitational stiffness in the lateral and yaw directions.

The proposed method is validated by applying it to a wheelset example cited in the literature. Comparable results are obtained using the proposed technique. The describing function method presented in the report is quite general and is applicable to dynamic models exhibiting severe non-linear characteristics in profile. Critical speed, frequency of limit cycles, gravitational force, effective conicity, gravitational stiffness and creepage, etc., can be easily computed using the proposed algorithm.

17. Key Words	18. Distribution Statement
Rail System Dynamics Describing Function Analysis Hunting	DOCUMENT IS AVAILABLE TO THE PUBLIC THROUGH THE NATIONAL TECHNICAL INFORMATION SERVICE, SPRINGFIELD, VIRGINIA 22161

19. Security Classif. (of this report)	20. Security Classif. (of this page)	21. No. of Pages	22. Price
Unclassified	Unclassified	102	

Form DOT F 1700.7 (8-69)

PREFACE

The Federal Railroad Administration is sponsoring research development and demonstration programs to provide improved safety, performance, speed, reliability and maintainability of rail transportation systems at reduced life cycle costs. A major portion of these efforts is related to improvement of the dynamic characteristics of rail vehicles and track structures.

Under the RR 515 Project, Transportation Systems Center is maintaining a center for resources to be applied to these programs. As part of this effort, TSC has been acquiring, developing and extending analysis tools to support these FRA objectives.

As a result of a survey of FRA requirements and existing analysis tools, it was found that there is a need for extension of the frequency domain linear analysis computer programs to include significant non-linearities without incurring the large cost associated with direct numerical integration of the equations of motion. This report represents an initial study in the applicability of the describing function approach used in control system analysis to predict the stability of rail vehicles.

The research effort described in this report was conducted by Professor Garg of Duke University while serving under a temporary appointment to the staff of Transportation Systems Center of the U.S. Department of Transportation.

The author wishes to acknowledge many helpful discussions held with Dr. Herbert Weinstock of the TSC and Professor Armand B. Perlman during the course of this research. Mr. Richard Gunzel provided programming support for the DEC System available at the Transportation Systems Center

TABLE OF CONTENTS

LIST OF ILLUSTRATIONS

V	Forward Speed of the Wheelset
V_{cr}	Critical Speed of the Wheelset
y	Lateral Displacement of the Axle
Y_l	Amplitude of Wheelset Lateral Oscillation
α	Tyre Profile Conicity
α_e^*	Describing Function of Effective Conicity
δ_o	Factor Dependent upon Track and Wheel Gage
ψ	Yaw Displacement
ω	Frequency of Sinusoidal Input to Nonlinearity
ω_k	Frequency of Kinematic Oscillations
$(\dot{})$	Represents Derivative with respect to Time
$(')$	Represents Derivative with respect to Lateral Displacement

1. INTRODUCTION

A significant amount of research effort in recent years has dealt with the problem of hunting of railway axles and trucks [B5, C2, D2, L3, M1, M2, R1, W1, W2].* Hunting in rail vehicles is a continuous lateral oscillation and may be termed as primary or secondary. Primary hunting refers to a strongly coupled lateral motion of car body and truck which usually takes place at low speeds. At higher speeds, lateral oscillations of trucks and axles take place in a coupled lateral and yawing mode. This phenomenum, known as secondary hunting, tends to limit the safe operating speeds of rail vehicles. Above critical speeds the secondary hunting leads to an excessive lateral motion, with wheel flanges banging from rail to rail and sometimes riding over the rail to cause vehicle derailment. Conventionally, in order to correct the situation, the vehicle is withdrawn from service and the wheels are machined to their original profile before being reintroduced in service.

Normally, the wheels are designed with a straight conical taper and a flange. However, after having been in operation for sometime the conical profile gets worn to a hollowed profile to conform to the railhead profile [W3]. The wheel profile turns into a continuous

---

* Numbers in square brackets designate references at the end of report.

curve, and during hunting of the wheelset axle the contact point moves laterally along these two profiles. When the amplitude of oscillations becomes excessive, one of the contact points moves way into the flange. For large amplitude oscillations it is conceivable that the wheel will ride the rail. An appropriately profiled wheel may prevent derailment.

While there is great interest in attaining high speeds for travel via rail vehicles, there are also various problems associated with high speed operation, including safety, stability, and wear. From a safety viewpoint, for example, it is necessary to limit the transverse efforts exerted by the vehicles onto the rails to values compatible with the lateral strength of the track. Also, tread wear is associated with a decrease in ride quality which leads to passenger discomfort. Lateral track elasticity is dependent upon factors such as rail head profile, tie spacing and torsional resistance of the track. The last factor is based upon the force required to secure the track to the ties and base plates. Furthermore, track elasticity deviates from its initial value during the track life time. The margin of safety from derailment is a function of track lateral stability. In the present analysis, in addition to several others, the effect of variation in track stiffness on vehicle critical speed is examined.

Dynamic analysis of rail-wheel interaction has been conventionally carried out using linear techniques. The results are valid for small perturbation from equilibrium point and for well maintained tracks [W1]. In actual practice, however, the rails may have

large vertical and lateral irregularities. In addition, the wheel profile may deviate from the initial conical configuration due to wheel wear after running for a certain length of time. As reported in the literature [B3,C2,D2,L2,M3,R1,W4], primarily the following approaches have been used for an evaluation of critical speeds and limit cycle analysis:

1) Small Perturbation Linearization

2) Numerical Integration Schemes

3) Krylov and Bogoliubov Method

A linearized analysis is valid only for small deviations from the equilibrium or operating point. Previous studies[C3,G2] have indicated that a linearized analysis of nonlinear equations predicts that below a critical or hunting speed any perturbations of motion from the equilibrium point simply decay. Above the hunting speeds, however, the oscillations grow subsequent to any deviations from the equilibrium states. The results derived on the basis of linearized analysis may not hold for large deviations and hence may not provide a realistic insight into the dynamic behavior of actual systems.

The dynamics of the rail-wheel interaction includes several nonlinear relationships which lead to a formulation of the model in terms of nonlinear dynamical equations. Integration of these equations to arrive at a temporal response can be carried out for the linearized equations or in their nonlinear forms using well-known numerical methods (for example, via a Runge-Kutta algorithm). To find the solutions as a function of time, one needs to specify

the initial condition for each state variable in terms of which the system equations are formulated. For the linear system, the transient response can be obtained for any set of initial conditions. For another set of initial conditions, one can expect to obtain similar dynamical behavior for the system; this is true, since in these cases the principles of superposition and homogeneity would hold.

To obtain the global or in-the-large behavior of the system in which the variables, such as the displacement of the wheel on the rail profile, may be allowed to have large deviations, the application of linear methods may yield erroneous results. This is true both qualitatively and quantitatively, since the nonlinearities may be important, and the linear analysis may fail to reveal their dynamic influence. Computer techniques for system simulation provide straightforward and realizable solution procedures and calculations for <u>any</u> set of given initial conditions. However, for a different set of initial conditions, the solution is to be carried out again, and unfortunately, in the case of nonlinear systems, the solution of the system under two sets of initial conditions may be vastly different. It is essential, therefore, that to obtain a global solution valid under all operating conditions, one would have to carry out a large number of numerical computational runs. This process can be excessively time consuming and prohibitively expensive due to the necessity of checking a large set of initial conditions. Even so, there is no guarantee that there does not exist <u>an</u> initial condition for which the behavior of the system will be very different from others.

Approximate methods have also been used for a variety of problems involving the analysis of nonlinear oscillations. Krylov and Bogoliubov method [B4] is one such technique, and it has been used for evaluating limit cycle oscillation amplitude of systems involving rail-wheel interactions. However, as is true for any approximate method, a significant associated problem is that of accuracy. A certain degree of assurance is necessary to guarantee the applicability of the method involved and ensure the validity of both qualitative and quantitative results. The method attributed to Krylov and Bogoliubov has been used to determine the oscillations of periodic response. The method also gives in evidence the transient process corresponding to small amplitude variations in oscillations. A major limitation of the technique, however, is that it is only applicable to systems described by second-order differential equations. Furthermore, the approach linearizes the nonlinear system, with the assumption that, in the neighborhood of the steady-state oscillations, the transient process approximates the transient response of an equivalent linear system with slowly varying amplitude and frequency.

A large number of practical nonlinear systems cannot be adequately described by a second-order nonlinear differential equation. The method of describing function, often called the method of harmonic linearization, is applicable to systems described by high-order nonlinear differential equations. This method is very commonly applied for stability analysis and investigation of sustained nonlinear oscillations, called limit cycles. The method was developed by Kochenburger in the U.S. [K2,G1] and is extensively used in connection

with problems of control system analysis.

The basic concept behind the describing function method is that first the given differential equations are reformulated in terms of an autonomous nonlinear feedback system, with the nonlinearity isolated from the linear portion of the system. It is of basic interest to determine whether the system can exhibit periodic oscillations. Furthermore, the stability of these oscillations can be obtained using the describing function technique.

To solve a problem using describing function analysis it is assumed that the input to the nonlinearity is a sinusoidal function of specific amplitude A and a constant frequency of oscillation ω. The requirements on the existence of an oscillatory solution are based on the filter hypothesis. This hypothesis implies that the distorted signal resulting as the output of the nonlinearity has the higher harmonics filtered out by the linear plant and only the fundamental frequency remains. This fundamental harmonic gives rise to the assumed oscillatory solution of the system. The postulation is quite realistic, since the nonlinear system may exhibit periodic oscillations arbitrarily close to a pure sinusoid. A describing function for a general nonlinearity may be assumed to correspond to a complex input amplitude and frequency-dependent transfer function.

There are certain applicability conditions on the nonlinear characteristic and linear portion of the system for the describing function analysis to be valid. These include the validity of generalized filter property of the system, which is easily satisfied if the linear part of the system is stable. If an oscillatory input

is applied to an unstable linear part of the system, the filter property has no meaning. The second applicability condition is that there should be no open-loop purely imaginary poles in the linear part of the system, i.e., the linear plant should be open-loop stable. Finally, the nonlinear function should have finite partial derivatives. This condition is satisfied by requiring the components of the describing function to be monotonic functions of amplitude A in the neighborhood of the value of A that corresponds to the actual periodic solution.

2. DYNAMIC EQUATIONS OF MOTION FOR THE SUSPENDED WHEELSET

For high speed hunting, car body and truck masses are effectively isolated from wheelset. Dynamic equations have been written for investigating the guidance and stability of complete vehicle models [C3], half-car models [W1], trucks [G2] and simple wheelsets [L1, W2]. In addition, experimental results have been reported [D1,M2], including their comparisons with the analytically obtained results. These experiments have been carried out on simple wheelset models, scaled vehicles, and conventional rail vehicles. Obviously, the more degrees of freedom included in the model, the more complex it becomes. Based upon such analyses one can optimize suspension designs, evaluate wheel-rail forces, vehicle displacement, velocity, and acceleration levels, and construct suitable control strategies to satisfy any predefined performance criteria, e.g., passenger comfort, or vehicle derailment. In addition it may be desirable to minimize wear between the wheels and guideway structure, and provide maximum adhesion for both traction and braking.

As pointed out above, many models, with varying degrees of sophistication, are generally available in the literature. For practical purposes relative to secondary hunting, however, a simplified suspended wheelset model is adequate to represent wheel-rail dynamics. The wheelset configuration is shown in Figure 2-1. It is assumed that the wheelset travels on a straight ideal track (no irregularities) with a velocity V. The profile of the wheels is considered to be

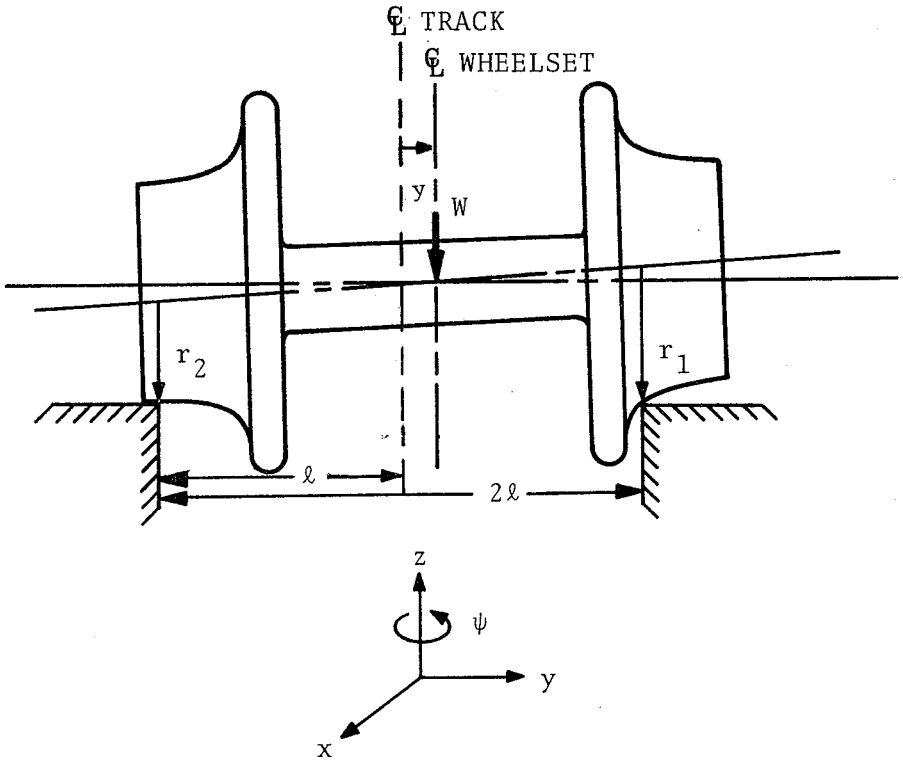

Figure 2-1. Schematic Representation of a Simple Wheelset on a Regular Track

nonlinear. Linear creep coefficients are assumed in the lateral and yaw directions,and the effect of spin creep is neglected.

The equations of motion for the wheelset can be derived on the basis of forces and moments acting between the worn wheels and the rail. The current practice is to use a conical profile on the new wheels; however, wear of the wheel surface during running leads to a hollowing of the wheel. Efforts are underway to experiment with new designs of wheel profiles [W3] in order to utilize the associated gravitational stiffness and improve wheelset stability.

The gravitational stiffness results from an elevation of the wheelset center caused by a lateral displacement of the wheelset. Obviously, the gravitational stiffness is a constant for conical wheels. For profiled wheels, however, it is a function of the rolling radii at the contact points and axle load.

Gravitational stiffness enters two places in dynamic equations. In the force equation it appears as the "lateral gravitational stiffness," which is defined as the variation in lateral force for each unit change of wheelset lateral displacement. In the moment equation it appears as the yaw gravitational stiffness,which is defined as the variation of net torque on the wheelset for each unit change in yaw displacement.

Profiled wheels have another characteristic, namely the effective conicity. For conical wheels it is the value of cone angle, and hence is a constant. For worn wheels the effective conicity is defined as that cone angle which for simply coned wheels would produce the same wavelength of kinematic oscillations (the natural oscillatory motion of a free wheelset rolling along the track) [G2].

Creep is basically the phenomenon of deviation from rolling [M4], which plays a critical role in the lateral instability of the wheelset. The pure rolling motion of a wheelset cannot be thus maintained due to the phenomenon of creep. There is a large body of literature available dealing with fundamental concepts related to creep, such as in References J1, J2, and V2. However, not much experimental data is available for creepage in full-scale vehicles. One of the reasons for this deficiency is the difficulty encountered in actual measurement of creep forces.

Linear relationships exist between creepage and tangential forces, and the creep coefficients are constants. These relationships hold for small deviations from rolling motion. As the creepages increase there is a marked deviation from linearity. Ultimately the wheels start to slide on the rail, and the limiting value of creep force is equal to coulomb friction force. This is shown in Figure 2-2.

In the present analysis the longitudinal and lateral creep coefficients are considered equal. The longitudinal creep force in the linear region is given by the product of longitudinal creep coefficient and the longitudinal creepage. A similar result holds for creep in the lateral direction. A typical empirical relationship is that the creep coefficient may be assumed to be 150 times the normal force.

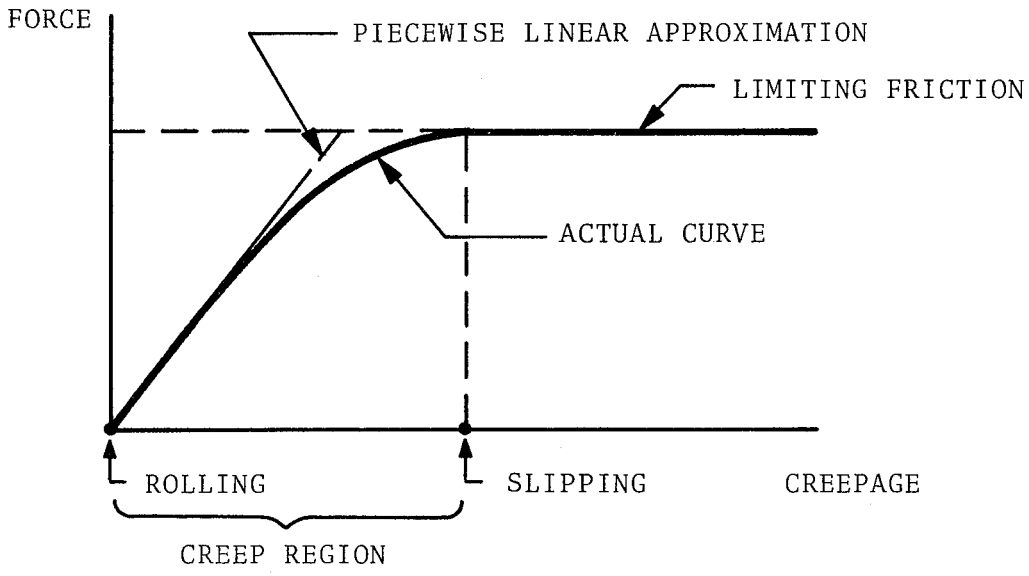

Figure 2-2. Creepage vs. Force in the Lateral and Longitudinal Directions

The dynamic equations of motion for the wheelset can be set up in terms of lateral displacement y and yaw displacement ψ of the wheelset relative to the track. Following the development given in section 3 of Reference [W1], the total force in the lateral direction is:

$$F_y = -2f_L(\frac{\dot{y}}{V} - \psi) - F_g - k_y y$$

where,

F_y = force in the lateral direction

f_L = lateral creep coefficient

y = lateral displacement

V = vehicle forward velocity

ψ = yaw displacement

F_g = Force due to gravitational stiffness

k_y = stiffness of the primary suspension

and

$$(\cdot) \triangleq \frac{d}{dt}$$

For an axle and wheelset of mass m, the total lateral force is given by

$$F_y = m\ddot{y}$$

and the equation of motion in the lateral direction becomes

$$m\ddot{y} + 2f_L(\frac{\dot{y}}{V} - \psi) + F_g + k_y y = 0$$

Reference [W1] uses a virtual work approach to derive the expression for F_g based upon the axle load W, half track gage ℓ, radii r_1, r_2 and their derivatives (with respect to lateral displacement y) as

$$F_g = \frac{W}{2\ell} (r_1 - r_2) + \frac{W}{2\ell} (r_1' - r_2') y_1 + \frac{W}{2} (r_1' + r_2')$$

where

(') indicates the first derivative of the rolling radius with respect to lateral displacement y.

The net torque applied by the rails on the wheelset according to Reference [W1] is

$$M = -2f_T\ell \left(\frac{\ell\dot{\psi}}{V} + \frac{r_1 - r_2}{r_1 + r_2}\right) + M_N - k_\psi \psi$$

where

f_T = tangential creep coefficient

r_1 = instantaneous rolling radius of the right wheel

r_2 = instantaneous rolling radius of the left wheel

M_N = destabilizing torque applied by normal forces

k_ψ = yaw stiffness of the primary suspension

The expression for the torque M_N based on Reference [W1] is:

$$M_N = \frac{W\ell}{2} (r_1' - r_2') \psi$$

Also, for a wheelset of moment of inertia C about the centroidal axis normal to the axle,

$$M = C\ddot{\psi}$$

Hence the dynamic equation of motion in the yaw direction is:

$$C\ddot{\psi} = -2f_T\ell \left(\frac{\ell\dot{\psi}}{V} + \frac{r_1-r_2}{r_1+r_2}\right) + \frac{W\ell}{2}(r_1'- r_2')\psi - k_\psi\psi$$

i.e.

$$C\ddot{\psi} + \frac{2f_T\ell^2}{V}\dot{\psi} + k_\psi\psi - \frac{W\ell}{2}(r_1'- r_2')\psi + 2f_T\ell\left(\frac{r_1-r_2}{r_1+r_2}\right) = 0$$

3. LINEARIZED ANALYSIS

The dynamic model of a wheelset moving along a straight track with a constant velocity V can be considered to have two degrees of freedom, one lateral and the other, yaw. For small amplitude motions the nonlinear equations can be linearized to yield the following set of equations:

$$m\ddot{y} + \frac{2f_L}{V}\dot{y} + k_y y = 2f_L\psi$$

and

$$C\ddot{\psi} + \frac{2f_T\ell^2}{V}\dot{\psi} + k_\psi\psi = -2f_T\frac{\alpha\ell}{r_o}y$$

where the various parameters have been defined previously.

For state variables y_1, y_2, y_3 and y_4:

$$y_1 = y$$
$$y_2 = \dot{y}$$
$$y_3 = \psi$$
$$y_4 = \dot{\psi}$$

the above set of equations can be represented in a matrix form given by

$$\frac{d}{dt}\begin{bmatrix} \dot{y}_1 \\ \dot{y}_2 \\ y_3 \\ y_4 \end{bmatrix} = \begin{bmatrix} 0 & 1 & 0 & 0 \\ \frac{-k_y}{m} & \frac{-2f_L}{Vm} & \frac{2f_L}{Vm} & 0 \\ 0 & 0 & 0 & 1 \\ \frac{-2f_T \ell \alpha}{r_o C} & 0 & \frac{-k_\psi}{C} & \frac{2f_T \ell^2}{VC} \end{bmatrix} \begin{bmatrix} y_1 \\ y_2 \\ y_3 \\ y_4 \end{bmatrix}$$

Since the equations have been linearized Laplace transform technique is applicable and the characteristic function can be obtained by evaluating the following determinant:

$$\begin{vmatrix} s & -1 & 0 & 0 \\ k_{Y/m} & (s+\frac{2f_L}{Vm}) & \frac{-2f_L}{Vm} & 0 \\ 0 & 0 & s & -1 \\ \frac{2f_T \ell \alpha}{r_o C} & 0 & \frac{k_\psi}{C} & s+\frac{2f_T \ell^2}{VC} \end{vmatrix}$$

The characteristic equation resulting from this above function is:

$$s^4 + 2\left(\frac{f_L}{mV} + \frac{f_T \ell^2}{VC}\right) s^3 + \left(\frac{k_\psi}{C} + \frac{k_y}{m} + \frac{4 f_T f_L \ell^2}{mCV^2}\right) s^2$$

$$+ 2\left(\frac{f_L}{Vm} \cdot \frac{k_\psi}{C} + \frac{k_y}{m} \frac{f_T \ell^2}{VC}\right) s$$

$$+ \left(\frac{k_y}{m} \cdot \frac{k_\psi}{C} + \frac{4 f_T f_L}{r_o mC} \ell\alpha\right) = 0$$

The parameters may be combined in accordance with the following definitions leading to a more convenient form of the above equation.

$$\beta^2 = r_o \ell/\alpha$$

$$\omega_k = V/\beta$$

$$\omega_\psi^2 = \frac{k_\psi}{C}$$

$$\omega_T^2 = \frac{2 f_T \ell^2}{C\beta}$$

$$\omega_L^2 = \frac{2 f_L}{m\beta}$$

$$\omega_y^2 = k_{y/m}$$

$$s_1 = s/\omega_k$$

In terms of above quantities the equation is:

$$\left(\frac{\omega_k^4}{(\omega_y^2 \omega_\psi^2 + \omega_T^2 \omega_L^2)}\right) s_1^4 + \left(\frac{\omega_k^2 (\omega_L^2 + \omega_T^2)}{(\omega_y^2 \omega_\psi^2 + \omega_T^2 \omega_L^2)}\right) s_1^3$$

$$+ \left(\frac{\omega_k^2 (\omega_\psi^2 + \omega_y^2) + \omega_\psi^2 \omega_L^2}{\omega_y^2 \omega_\psi^2 + \omega_T^2 \omega_L^2}\right) s_1^2$$

$$+\left(\frac{\omega_L^2\omega_\psi^2 + \omega_T^2\omega_y^2}{\omega_y^2\omega_\psi^2 + \omega_T^2\omega_L^2}\right) s_1 + 1 = 0$$

Routh-Hurwitz criterion [M6] may be applied to the characteristic function to arrive at the stability limit for the linearized dynamical model of the wheelset. For the above polynomial the critical frequency ω_k, for hunting can be derived from the condition:

$$B_1(B_3B_2 - B_4B_1) - B_3^2 B_o = 0$$

where

$$B_4 = \frac{\omega_k^4}{(\omega_y^2\omega_\psi^2 + \omega_T^2\omega_L^2)}$$

$$B_3 = \frac{\omega_k^2(\omega_L^2 + \omega_T^2)}{(\omega_y^2\omega_\psi^2 + \omega_T^2\omega_L^2)}$$

$$B_1 = \frac{\omega_k^2(\omega_\psi^2 + \omega_y^2) + \omega_T^2\omega_L^2}{(\omega_y^2\omega_\psi^2 + \omega_T^2\omega_L^2)}$$

and

$$B_o = 1$$

An algebraic manipulation of the above quantities in terms of the stated condition yields

$$\omega_k^2 = \frac{\omega_\psi^2 + \left(\frac{\omega_T^2}{\omega_L^2}\right)\omega_y^2}{\left(1 + \frac{\omega_T^2}{\omega_L^2}\right)\left(1 - \frac{(\omega_\psi^2 - \omega_y^2)^2}{(\omega_L^2 + \omega_\psi^2)^2}\right)}$$

The frequency of kinematic oscillations ω_k, corresponds to the critical speed V_{cr} such that the amplitude of oscillations would continue to grow exponentially with time above this speed; below this speed the small oscillations will decay.

It should be noted that the Routh-Hurwitz test cannot be straightforwardly applied to the nonlinear dynamical model for stability analysis. In case of nonlinear systems, there is the additional concept of limit cycling mode. Linear systems do not exhibit limit cycles, and to handle the nonlinear problem a modified approach must be used. The describing function method provides the answer, as will be discussed in section 4.

4. THE DESCRIBING FUNCTION APPROACH FOR LIMIT CYCLE ANALYSIS

The describing function method of nonlinear analysis involves the replacement of the nonlinear element by its "equivalent" linear representation,which is an input amplitude dependent function. Each describing function is dependent upon the assumed input to the nonlinear element. Typically, the input is considered to be a sinusoid of amplitude A and frequency ω, and the corresponding describing function is called a sinusoidal input describing function. The input to the nonlinearity is not restricted to a sinusoid. Other types of inputs have also been used to derive describing function expressions. These include two sinusoids [A1], a bias and a sinusoid [O1], three simultaneous inputs [V1], and a gaussian input [A2]. In the analysis presented in this report, a sinusoidal input describing function approach has been applied for stability and limit cycle.

The sinusoidal input describing function is derived from the consideration of harmonic response of a nonlinearity to a sinusoidal input at various frequencies and amplitudes. The output will be a nonsinusoidal periodic waveform with the same period as the input wave. The output wave will consist of a fundamental component and other higher harmonics. A sinusoidal input describing function is defined as the complex ratio of the fundamental component of the output to the input. The output is the product of describing function and the input and is dependent upon the input amplitude.

For all practical purposes a sinusoidal input describing function may be considered to be an equivalent linear operator which minimizes the mean-square difference between the actual output and its approximation based upon the fundamental components of the output waveform.

Consider a nonlinear input-output relationship

$$z = h(x)$$

where z is the output dependent on x, the input to the nonlinearity. If the nonlinear function is approximated by its describing function, and x is a sinusoidal input given by:

$$x = A \sin \omega t$$

A being the amplitude and ω the frequency of the sinusoidal input, then the error e is evaluated from:

$$\begin{aligned} e &= z_{actual} - z_{approximate} \\ &= h(x) - G^*(A)x \\ &= h(A \sin \omega t) - G^*(A) A \sin \omega t \end{aligned}$$

where $G^*(A)$ is the describing function for the nonlinear characteristic. For nonphase-shifting nonlinearities, as in the case considered, here, $G^*(A)$ is simply a function of input amplitude, and the describing function in these cases can be considered to be an amplitude dependent gain.

The linearizing gain $G^*(A)$ can be calculated from the basic property of the describing functions in terms of a minimization of mean-squared approximation error. The mean-squared error is given by

$$\bar{e}^2 = \frac{\omega}{2\pi} \int_0^{\frac{2\pi}{\omega}} e^2(t)\, dt$$

and the describing function G*(A) is obtained from the condition

$$\frac{\partial \bar{e}^2}{\partial G^*(A)} = 0$$

It was pointed out earlier (Section 1) that while the wheel profile may be initially conical, it wears to a hollow profile, leading to body hunting and a decrease in ride comfort. Design techniques are being evolved that would enable vehicles to be designed for stable operation on hollow tire profiles.

If the wheel-profile has an arbitrary shape the rolling radii r_1 and r_2 can be described by the following expressions [W1]:

$$r_1 = r_o + g(y_1 + \delta_o) - g(\delta_o)$$

$$r_2 = r_o + g(\delta_o - y_1) - g(\delta_o)$$

Here r_o is the nominal radius, and δ_o is a factor dependent on the wheel gage, track gage and the wheel and rail profiles. The lateral displacement is given by y_1 and g(v) represents a nonlinear polynomial function representing the profile

$$g(v) = \sum_{n=0}^{N} a_n v^n$$

With a suitable choice of axes the term δ_o can be set equal to zero. This set of axes is coincidental with the base and measuring lines on the tyre profiles. The value of N used in the present study ranged from 16 to 21, depending upon the specific tire profile. The procedure to arrive at the value of N was to

first select the profile. The discrete data from the profile were fed into a digital computer program called FITIT developed for the DEC-10 system available at the TSC . This program fits polynomials of varying degrees through the given set of data in a least-squares sense and computes the associated coefficients of the polynomial. The profile using the computed coefficients was graphically displayed via a CALCOMP plotter. Appendix A shows the various profiles used, computer plots for the profiles and the computed coefficients. For each of these profiles is also appended a plot of difference in rolling radii of opposite wheels as a function of lateral displacement.

There are three predominant nonlinearities in the dynamical equations derived for the wheelset. These include the gravitational stiffness in the lateral and the yaw directions, and the effective conicity. Each one of the three nonlinearities arises from the fact that the tire profile itself is nonlinear. In the following paragraphs the describing functions for these nonlinearities will be derived.

The expression for the gravitational force (valid up to N=21) in terms of the axle load W, half track gage ℓ, least-squares fit polynomial coefficients $a_o, a_1, \ldots, a_{21}$, and lateral displacement y, is:

$$F_g = \frac{W}{\ell} \{2(a_1 + a_2\ell)y_1 + 4(a_3 + a_4\ell)y_1^3$$
$$+ 6(a_5 + a_6\ell)y_1^5 + 8(a_7 + a_8\ell)y_1^7$$
$$+ 10(a_9 + a_{10}\ell)y_1^9$$
$$+ 12(a_{11} + a_{12}\ell)y_1^{11}$$
$$+ 14(a_{13} + a_{14}\ell)y_1^{13}$$
$$+ 16(a_{15} + a_{16}\ell)y_1^{15}$$
$$+ 18(a_{17} + a_{18}\ell)y_1^{17}$$
$$+ 20(a_{19} + a_{20}\ell)y_1^{19}$$
$$+ 21\ a_{21}y_1^{21}\}$$

Assuming that a sinusoidal input $y_1 = Y_1 \sin \omega t$ is available at hunting with Y_1 as the amplitude of limit cycle, the gravitational force can be represented by:

$$F_g = K_g^*(Y_1)y_1$$

where $K_g^*(Y_1)$ is the describing function for the lateral gravitational stiffness. Using the basic definition, the describing function can be obtained by minimizing the mean-squared error $\bar{e}^2$ given by

$$\bar{e}^2 = \frac{\omega}{2\pi} \int_o^{2\pi/\omega} (K_g^* y_1 - F_g)\, dt$$

which on setting $y_1 = Y_1 \text{Sin}\omega t$ and

$$\frac{\partial \bar{e}^2}{\partial K_g^*} = 0$$

leads to:

$$K_g^*(Y_1) = \frac{W}{\ell} \{2(a_1 + a_2\ell) + 4(a_3 + a_4\ell)(3/4)Y_1^2$$
$$+6(a_5 + a_6\ell)(15/24)Y_1^4$$
$$+ 8(a_7 + a_8\ell)(105/192)Y_1^6$$
$$+ 10(a_9 + a_{10}\ell)(945/1920)Y_1^8$$
$$+12(a_{11} + a_{12}\ell)(10395/23040)Y_1^{10}$$
$$+14(a_{13} + a_{14}\ell)(135135/322560)Y_1^{12}$$
$$+ 16(a_{15} + a_{16}\ell)(2027025/5160960)Y_1^{14}$$
$$+ 18(a_{17} + a_{18}\ell)(34459425/92897280)Y_1^{16}$$
$$+ 20(a_{19} + a_{20}\ell)(6.5472907/18.579456)Y_1^{18}$$
$$+ 21\ a_{21}\ (1.3749309/4.0874803)Y_1^{20}\}$$

The describing function above is valid not only for the periodic solution but also yields information about the transient process during the establishment of the corresponding sustained oscillations. As a result the stability of the limit cycle can be investigated using the describing function technique.

The yaw gravitational stiffness, K_a , is obtained from a consideration of the destabilizing torque due to normal forces, which is given by:

$$M_N = \frac{W\ell}{2} [g'(y_1 + \delta_o) - g'(\delta_o - y_1)]\ \psi$$
$$= K_a(y)\psi$$

Assuming $K_a^*(Y_1)$ to be the describing function for the gravitational yaw stiffness K_a, one can obtain an expression for K_a^* by minimizing the mean squared error as in the case of lateral gravitational stiffness. The yaw gravitational stiffness describing function K_a^* is:

$$\begin{aligned} K_a^*(Y_1) = W\ell \; \{ & a_1 + 3a_3\,(1/2)\,Y_1^2 \\ & + 5a_5\,(3/8)Y_1^4 \\ & + 7a_7\,(15/48)Y_1^6 \\ & + 9a_9\,(105/384)Y_1^8 \\ & + 11a_{11}(945/3840)Y_1^{10} \\ & + 13a_{13}(10395/46080)Y_1^{12} \\ & + 15a_{15}(135135/645120)Y_1^{14} \\ & + 17a_{17}(2027025/10321920)Y_1^{16} \\ & + 19a_{19}(3.4459425/18.579456)Y_1^{18} \\ & + 21a_{21}(0.65472907/3.7158912)Y_1^{20}\} \end{aligned}$$

Effective conicity is one of the most important factors governing the stability of the wheelset. It is defined as the simple coning angle which will produce the same wavelength of kinematic motion as the worn tires [K1]. The difference in rolling radii for a pair of wheels as a function of lateral displacement y_1 is given by:

$$r_1 - r_2 = \sum_{n=1}^{N} a_n (y_1)^n - \sum_{n=1}^{N} a_n (-y_1)^n$$

Based on the differential equations derived earlier, the effective conicity α_e is given by

$$\alpha_e = \frac{r_o}{y_1}\left(\frac{r_1 - r_2}{r_1 + r_2}\right)$$

$$\simeq \frac{r_o}{y_1}\frac{r_1 - r_2}{-2r_o}$$

$$= \left(\frac{r_1 - r_2}{2y_1}\right)$$

If α_e^* represents the describing function of the effective conicity α_e, then the error e is given by:

$$e = \alpha_e(y_1) - \alpha_e^*$$

and the mean squared error $\bar{e}$ is defined from:

$$\bar{e}^2 = \frac{\omega}{2\pi}\int_o^{2\pi/\omega} (\alpha_e(y_1) - \alpha_e^*)^2 dt$$

For a limit cycle oscillation of the wheelset with Y_1 as the amplitude of oscillation, the describing function α_e^* may be evaluated from:

$$\frac{\partial \bar{e}^2}{\partial \alpha_e^*} = 0$$

Proceeding as before gives the describing function for effective conicity $\alpha_e^*(Y_1)$ as:

$$\alpha_e^*(Y_1) = a_1 + a_3(1/2)\ Y_1^2 + a_5(3/8)\ Y_1^4 + a_7(15/48)\ Y_1^6 + a_9(105/384)\ Y_1^8 + a_{11}(945/3840)\ Y_1^{10} + a_{13}(10395/46080)\ Y_1^{12} + a_{15}(135135/645120)\ Y_1^{14} + a_{17}(2027025/10321920)\ Y_1^{16} + a_{19}(0.34459425/1.8579456)\ Y_1^{18} + a_{21}(0.65472907/3.7158912)\ Y_1^{20}$$

The hunting frequency ω_k for the wheel set and the critical speed V_{cr} are related by the expression

$$V_{cr} = \beta_e \cdot \omega_k$$

where the parameter β_e is given by:

$$\beta_e = \sqrt{r_o \ell / \alpha_e^*} \ .$$

The describing function terms may be introduced in the expression for ω_k to calculate the hunting frequency. Thus

$$\omega_k^2 = \frac{\omega_{\psi_e}^2 + \left(\frac{\omega_T}{\omega_L}\right)^2 \omega_g^2}{\left(1 + \frac{\omega_T^2}{\omega_L^2}\right)\left[1 - \frac{\left(\omega_{\psi_e}^2 - \omega_g^2\right)^2}{\left(\omega_L^2 + \omega_T^2\right)^2}\right]}$$

where,

$$\omega_{\psi_e}^2 = \frac{K_\psi - K_a^*}{C}$$

$$\omega_T^2 = \frac{2f_T \ell^2}{C\beta_e}$$

$$\omega_L^2 = \frac{2f_L}{m\beta_e}$$

$$\omega_g^2 = \omega_y^2 + \omega_{gf}^2$$

$$= \frac{k_y}{m} + \frac{k_g^*}{m}$$

$$\beta_e^2 = \frac{r_o \ell}{\alpha_e^*}$$

and

$$V_{cr} = \beta_e \omega_k$$

It should be noted that since α_e^* is a function of Y_1, β_e is also a function of Y_1. Consequently, ω_T and ω_L are dependent on Y_1. Similarly, K_a^* and K_g^* are functions of Y_1. Hence, ω_{ψ_e}

and ω_g are contingent upon the value of Y_1. This observation leads to the formulation of a computational scheme for generating pairs of ω_k and Y_1 values.

A possible computational scheme is to first assume a value for Y_1 and compute the values of K_g^*, K_a^*, and α_e^* since their describing function expressions depend upon Y_1. Next β_e may be calculated. With these results, evaluations may be made of ω_{ψ_e}, ω_T, ω_L, ω_{g_f}, ω_y and ω_g using the parametric values for the given wheelset. Every term in the expression for ω_k^2 is known with these computations. The critical speed V_{cr} may be obtained from the ω_k - β_e relationship. The value of Y_1 may be iterated next and the preceding computations repeated to yield another ω_k - Y_1 pair.

5. APPLICATION OF THE PROPOSED TECHNIQUE

The describing function method proposed in the previous chapter was applied to a problem dealing with the nonlinear dynamics of a railway vehicle wheelset [L2]. The motivation was to investigate the applicability of the proposed approach and to compare the results with the ones available in the literature. The values obtained using the technique advanced in this report compared favorably with the results reported elsewhere. In addition, the method is general and applicable to systems of higher order, a distinct advantage over the Krylov and Bogoliubov method.

The dynamic model in Reference L2 is set up in terms of generalized coordinates and nondimensionalized parameters. Curved wheel profile is one nonlinearity, and wheel-rail flange force is another. The force is of a dead-zone type, the clearance between the wheel flange and the rail representing one-half the deadband. The rails are assumed to be horizontal, straight and devoid of any irregularities. Linear creep is used in the dynamic model. The difference in rolling radii between the two wheels is approximated by a cubic polynomial.

The following equivalence may be established between the dimensional symbols used in Reference L2 and in the present analysis.

Variable/Parameter Name	Reference L2	This Report
Wheelset Moment of Inertia	I_2	C
Creep Coefficients	f	f_L, f_T
Suspension Lateral Stiffness	k_x	k_y
Suspension Yaw Stiffness	k_θ	k_ψ
One half track gage	a	ℓ
Lateral displacement	x	y
Yaw displacement	θ	ψ

Simulations were run for the parametric values reported in Reference L2. Figure 5-1 is a plot for the case $a_1 = 15.84$ shown in Figure 7 of Reference L2. The continuous curve shows several points translated from Law and Brand results (in terms of dimensional parameters) as identified by inverted triangles. The results obtained using the approach presented in this report are identical to those obtained by Law and Brand.

Appendix B has a complete listing of the program used for computations and a plot of the four curves which correspond to the four cases shown by Law and Brand in Figure 7 of their paper.

The equivalence between the variables and parameters used in the present analysis and those used in Reference L2 was established as follows. For $\delta_0 = 0$, and a cubic polynomial, the difference in rolling radii is given by the equation:

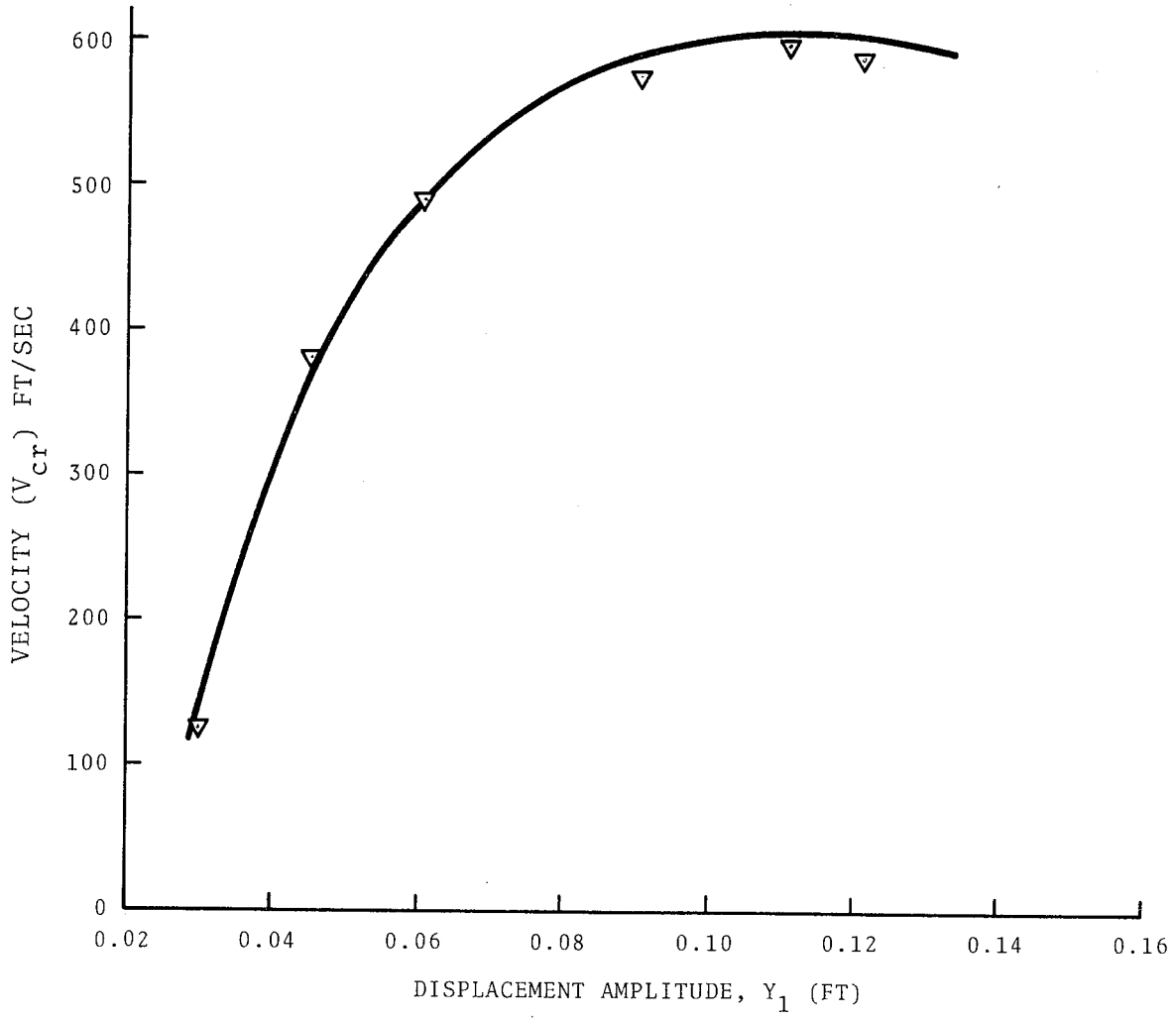

Figure 5-1. Comparison of Results Obtained by Using the Proposed Approach with Prior Results

$$r_1 - r_2 = 2(a_1 y_1 + a_3 y_1^3)$$

From analysis of Reference L2,

$$\phi = \frac{r_L - r_R}{2a}$$

$$= \bar{a}_0 \, q_1 + \bar{a}_1 q_1^{\,3}$$

$$= \bar{a}_0 \left(\frac{x}{a}\right) + \bar{a}_1 \left(\frac{x}{a}\right)^3$$

$$= \left(\frac{\bar{a}_0}{a}\right) x + \left(\frac{\bar{a}_1}{a^3}\right) x^3$$

Hence:

$$r_L - r_R = 2a\left\{\left(\frac{\bar{a}_0}{a}\right) x + \left(\frac{\bar{a}_1}{a^3}\right) x^3\right\}$$

$$= 2\left(\bar{a}_0 x + \frac{\bar{a}_1}{a^2} x^3\right).$$

The value of a_1 in present analysis equals a_0 used in Reference L2, and the value of a_3 is computed as the ratio (a_1/a^2). The equivalent values of this parameter corresponding to the four curves shown in Figure B-1 in Appendix B are, respectively, 0, 0.6336, 1.2672, and 2.5344.

6. DISCUSSION OF RESULTS

The approach advanced in this report was applied to three types of wheel profiles: a new conical profile with flange, a worn tread with an originally conical profile, and a wheel with a cylindrical profile. These three profiles are illustrated in the plots given in Appendix A. The conical wheel had a taper of 1 in 20 and corresponds to a standard profile for passenger trains as recommended by the Association of American Railroads (AAR). Similarly, the cylindrical profile was based upon the AAR specifications. The profile of a worn wheel resulted as a deviation from a standard conical wheel such that the maximum wear was on the wheel tread.

The approach employing the describing function techniques as outlined in section 4 was used to arrive at the results presented in this section. The following parameters were chosen as a base case for a typical wheelset.

Parametric variations were made from the following base values to investigate system sensitivity:

m, wheelset mass = 90 slugs (2,810 lb)

C, wheelset moment of inertia = 360 lb-ft-sec^2

k_y, primary suspension lateral stiffness = 5×10^4 lb/ft

k_ψ, primary suspension yaw stiffness = 1×10^5 lb-ft/rad

f_T, tangential creep coefficient = 4×10^5 lb

f_L, lateral creep coefficient = 4×10^5 lb

r_o, centered wheel rolling radius = 1.5 ft

ℓ, half of the track gage = 2.5 ft

For the above parameters, in the case of a wheel with straight conical profile (i.e., straight taper of 1 in 20 and no flanges) the linear analysis predicted a critical velocity of 184.26 ft/sec and a kinematic hunting frequency of 21.27 rad/sec. As will be evident from the following discussion, an inclusion of nonlinear profile in the analysis lowers the prediction of critical speed to a more realistic value.

The effect of static load on critical speed as a function of limit cycle amplitude is shown in Figure 6-1. A conventional conical tyre profile is used. Two plots are presented, one for the axle mass m, and the other for an additional weight of 20,000 lb on the axle. It is observed from the two plots that an increase in weight on the axle raises the peak value of critical velocity. Also the peak is shifted to the right for a higher load on the axle. This indicates that for the same limit cycle oscillation amplitude, there is an increase in critical speed; hence an increase in axle load has a stabilizing influence on the wheelset.

Figure 6-2 shows a comparison of $V_{cr} - Y_1$ plots for a new conical profile and a wheel with a tread worn profile. While the exact shape of the worn wheel curve will depend on the wear pattern of the profile, the general nature of the two curves is likely to be similar. Since most of the wear is on the tread portion of the conical profile, there is a marked difference between the values of critical velocity for the two cases. For larger oscillation amplitudes which

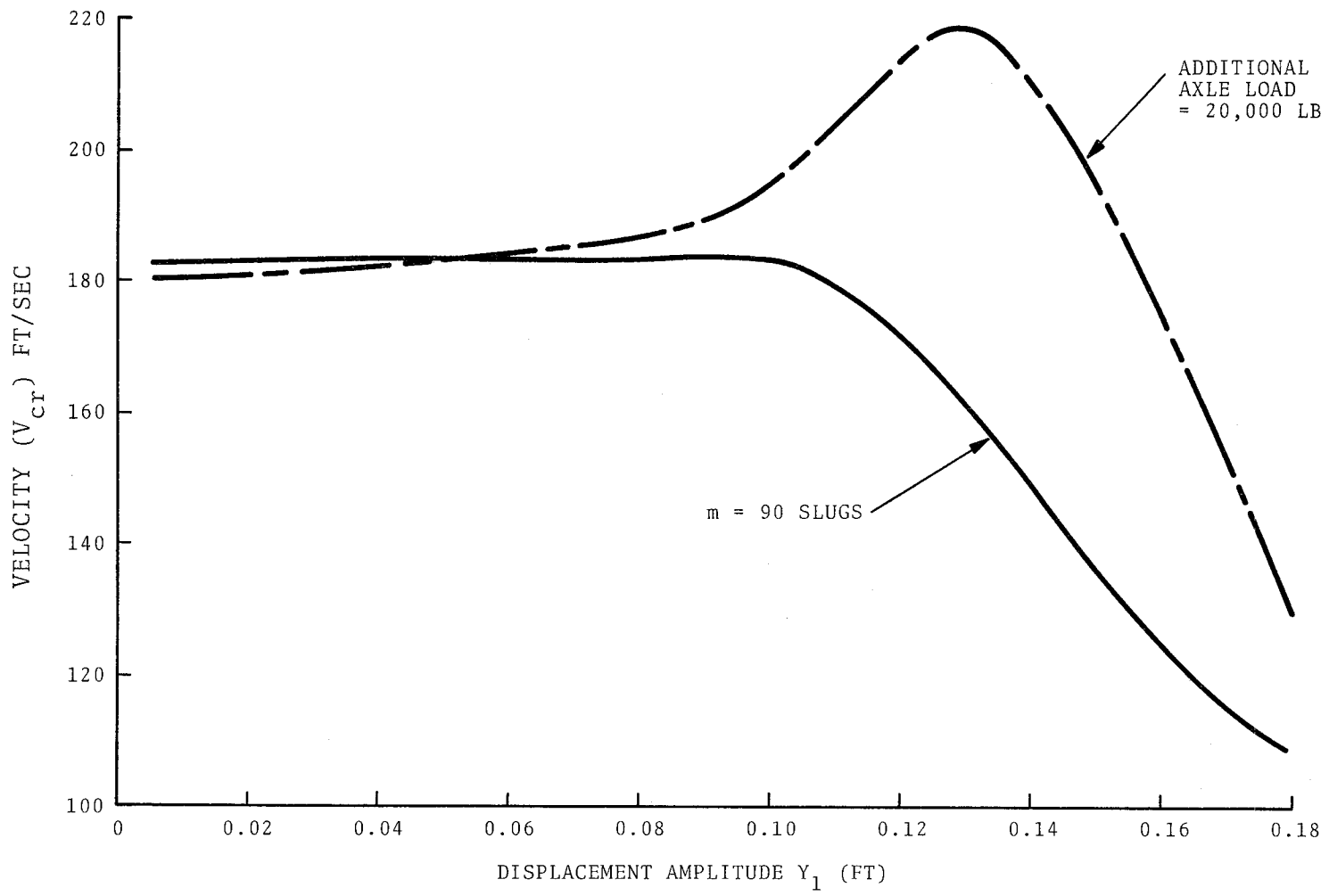

Figure 6-1. Effect of Change in Axle Load on Critical Velocity for a New Wheel with a Conical Profile

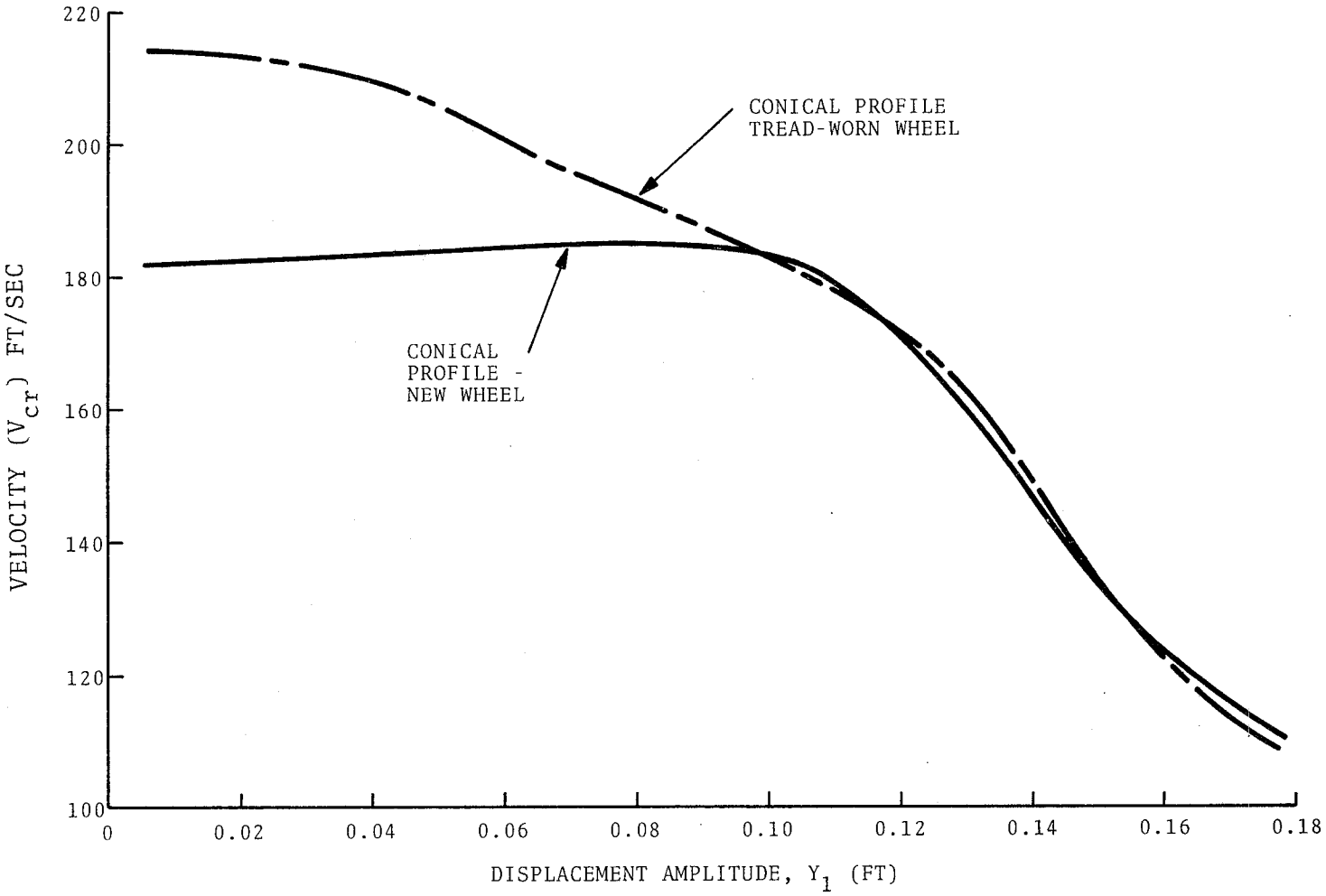

Figure 6-2. Critical Velocity vs. Amplitude of Limit Cycle Oscillation for the New and Tread Worn Conical Profile Wheels

correspond to the flange portion, the two curves are identical. Figure 6-3 shows the V_{cr} - Y_1 plots for the cylindrical profile wheel. It is noted that in this case the peak critical velocity is much higher than the previous two cases.

The influence of a change in k_y, the lateral stiffness of the primary suspension, is shown in Figure 6-4. This and all the succeeding plots are for the case of new wheel with a conical profile. Similar plots were generated for the remaining cases of tread-worn and cylindrical profiles, and it was found that the general nature of plots in the three cases was essentially similar. For the case illustrated in Figure 6-4, the yaw stiffness of the primary stiffness was maintained at a constant value of $k_\psi = 1 \times 10^5$ lb-ft/rad and the lateral stiffness was varied over values ranging from 2,000 lb/ft to 100,000 lb/ft. It was found that the critical speed was increased with an increase in k_y value. For example, a ten fold increase in lateral stiffness more than doubled the value of peak critical speed. It would seem attractive to use a high value of primary suspension lateral stiffness. However, a compromise value has to be chosen in view of ride comfort and other practical design considerations.

The effect of variation in k_ψ, the yaw stiffness of primary suspension, with the lateral stiffness held constant is shown in Figure 6-5. Again, as in the previous case, the critical speed increases with an increase in yaw stiffness. The lateral stiffness was fixed at 50,000 lb/ft and yaw stiffness ranged from 50,000 lb-ft/rad to 500,000 lb-ft/rad. For a ten-fold increase in yaw stiffness, the critical speed increased more than fifty percent. The limiting value of k_ψ is, however, dictated by wear and other operational considerations on curved tracks. A large value of yaw stiffness leads to

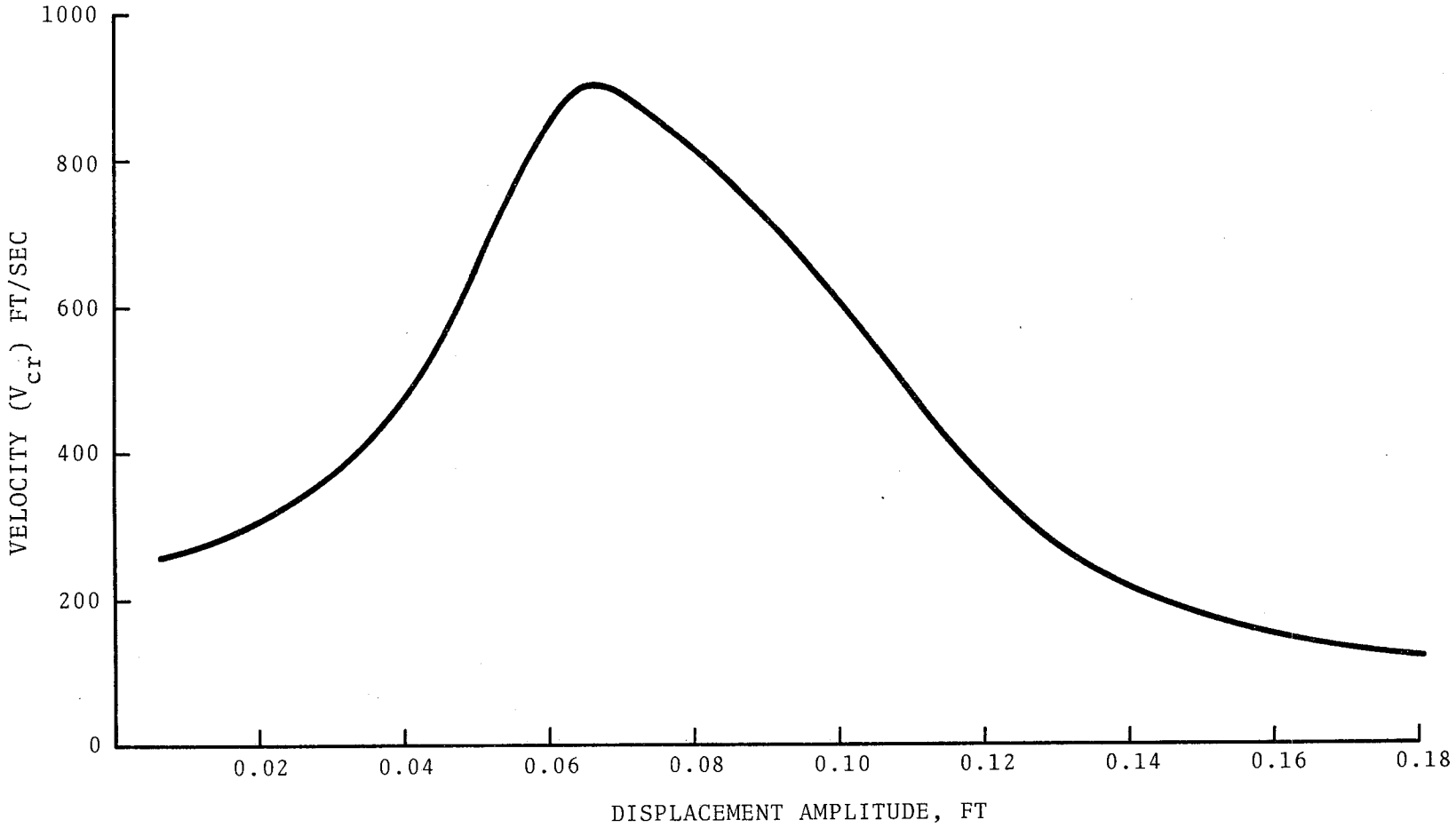

Figure 6-3. Critical Velocity vs. Limit Cycle Oscillation Amplitude for the Cylindrical Profile Wheelset

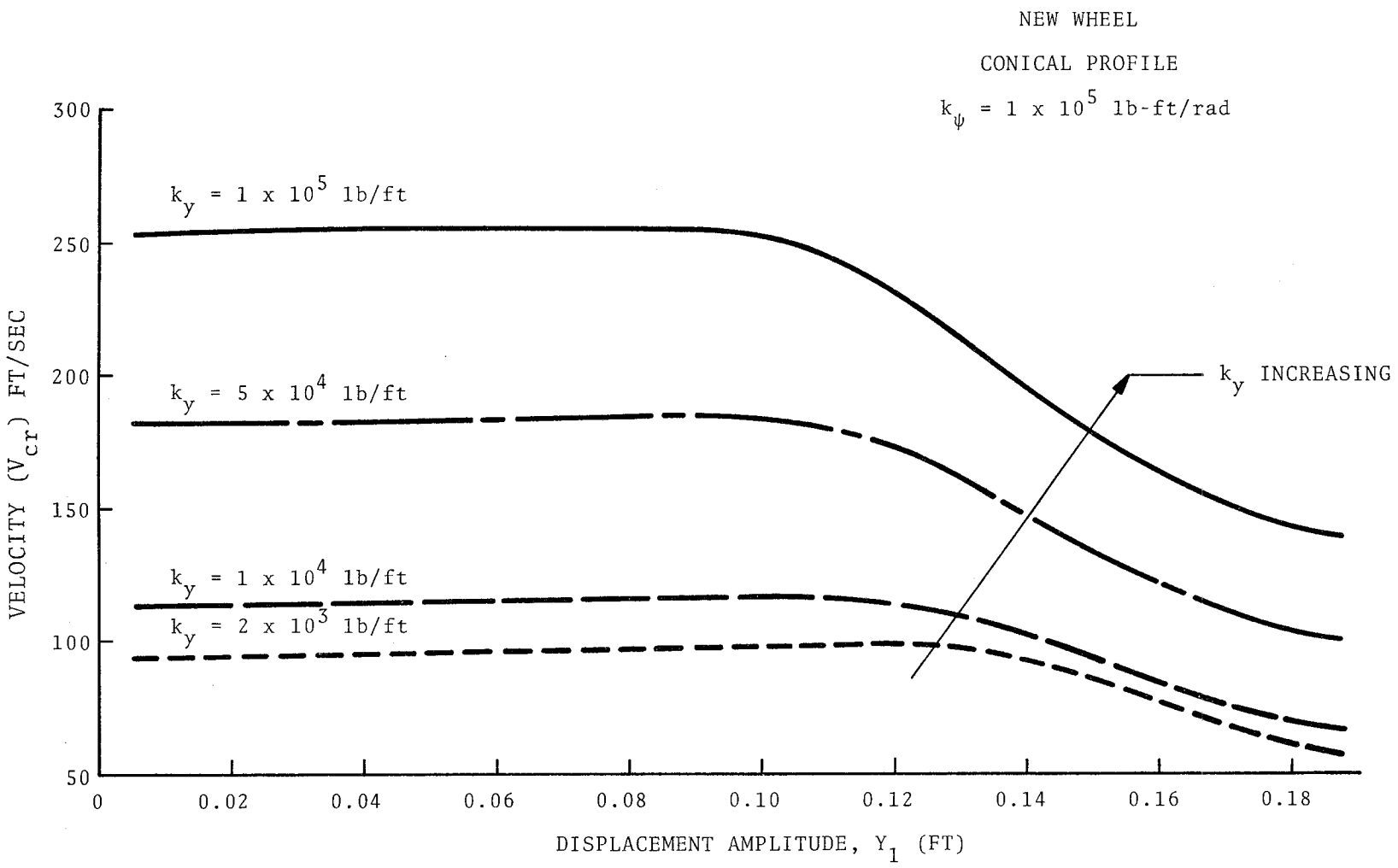

Figure 6-4. Effect of Variation in Primary Suspension Lateral Stiffness on Critical Speed of the Wheelset

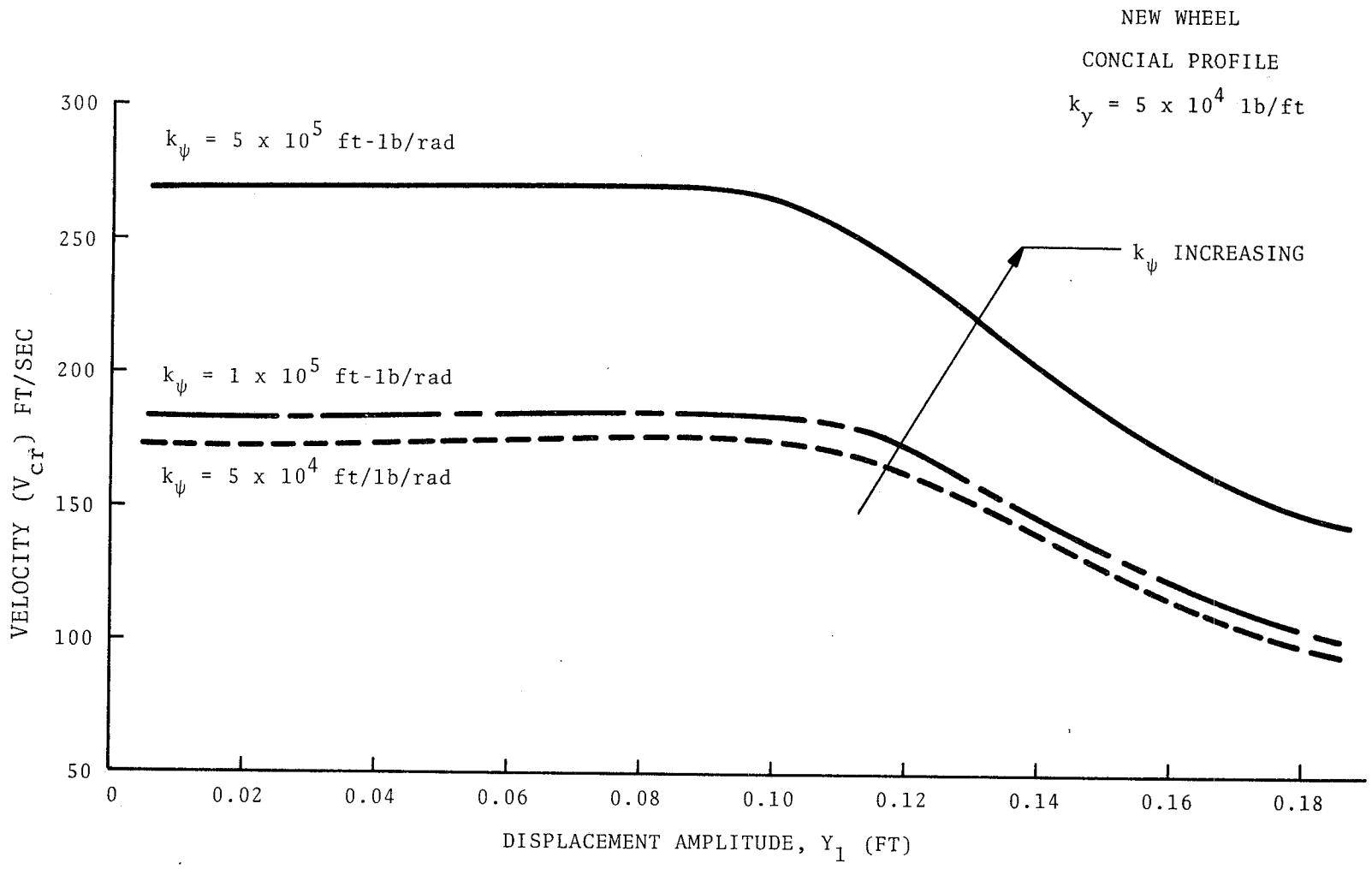

Figure 6-5. Effect of Variation in Yaw Stiffness of Primary Suspension on Critical Speed

increased wear on both flange and rail head while curving, and enhances the possibility of derailment [C2]. Based upon Figures 6-4 and 6-5, one can observe that one method of designing a vehicle for stable operation at high speeds is to use high values of lateral and yaw stiffness for primary suspensions.

The influence of change in creep coefficient on the critical speed is shown in Figure 6-6. In this case the value of m is held constant at 90 slugs. The creep coefficients chosen range from $1x10^5$lb to $4x10^6$ lb, and thus include a wide latitude of values resulting from a variety of surface conditions and operational forces. While there is a slight increase in critical speed with a decrease in creep coefficient, this increase takes place only at small values of creep coefficient. In addition, the magnitude of this increase is rather insignificant.

Figure 6-7 shows the effect of change in wheelset mass, m, on the peak critical speed of the wheelset. Each point identified on the curve corresponds to the peak critical speed for that mass value. The lateral and longitudinal creep coefficients f_L and f_T, respectively, were both held at a constant value of $4x10^5$ lb. It will be noted from the plot that the peak critical velocity increased as the wheelset mass decreased. Also, this increase is considerably higher than obtained with a decrease in creep coefficient. Thus, it is possible to attain higher stable running speeds with light weight wheelsets if all other parameters are held constant. However, manufacturing and strength considerations would dictate the specific choice of lower limit on the wheelset mass m.

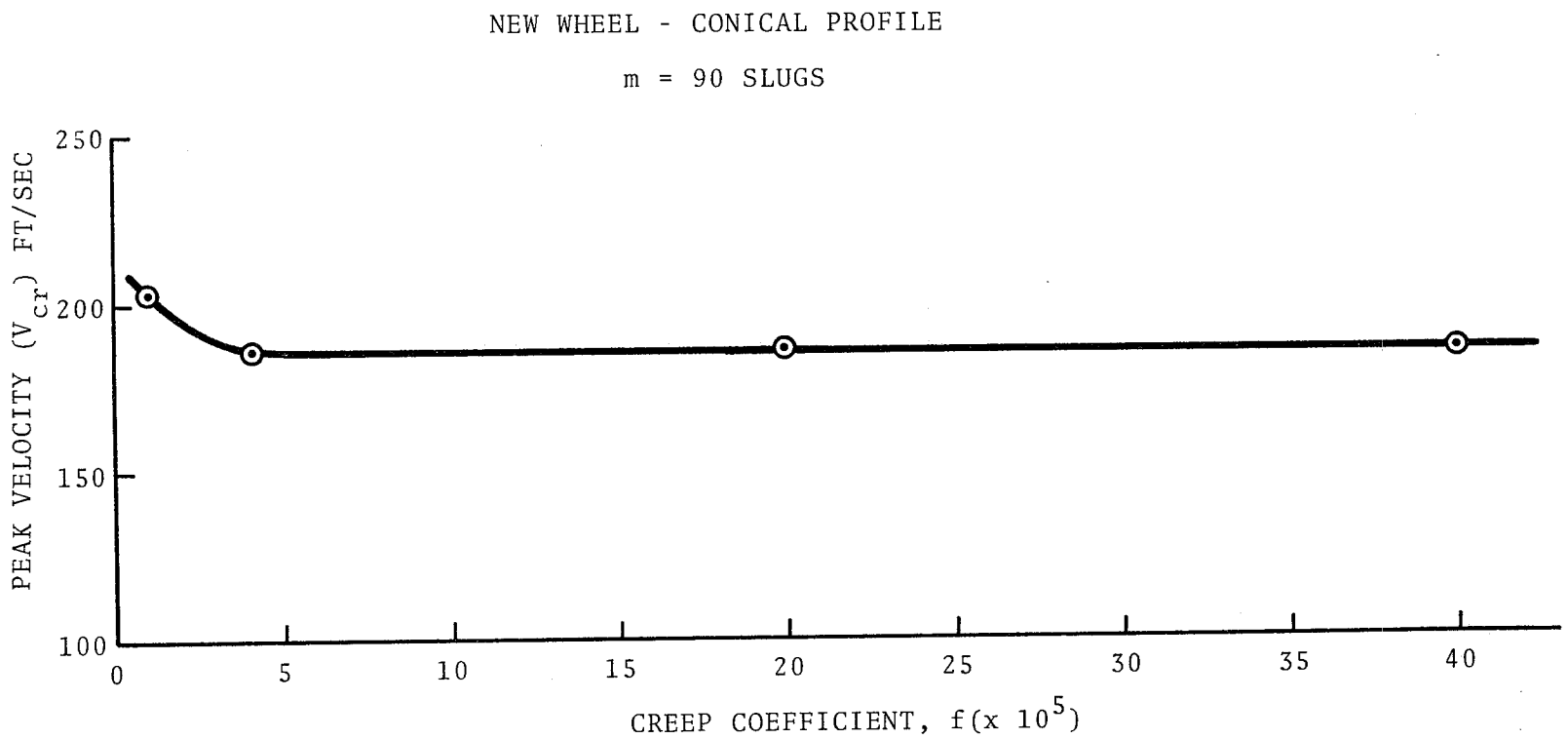

Figure 6-6. Variation of Critical Speed with a Change in the Creep Coefficient

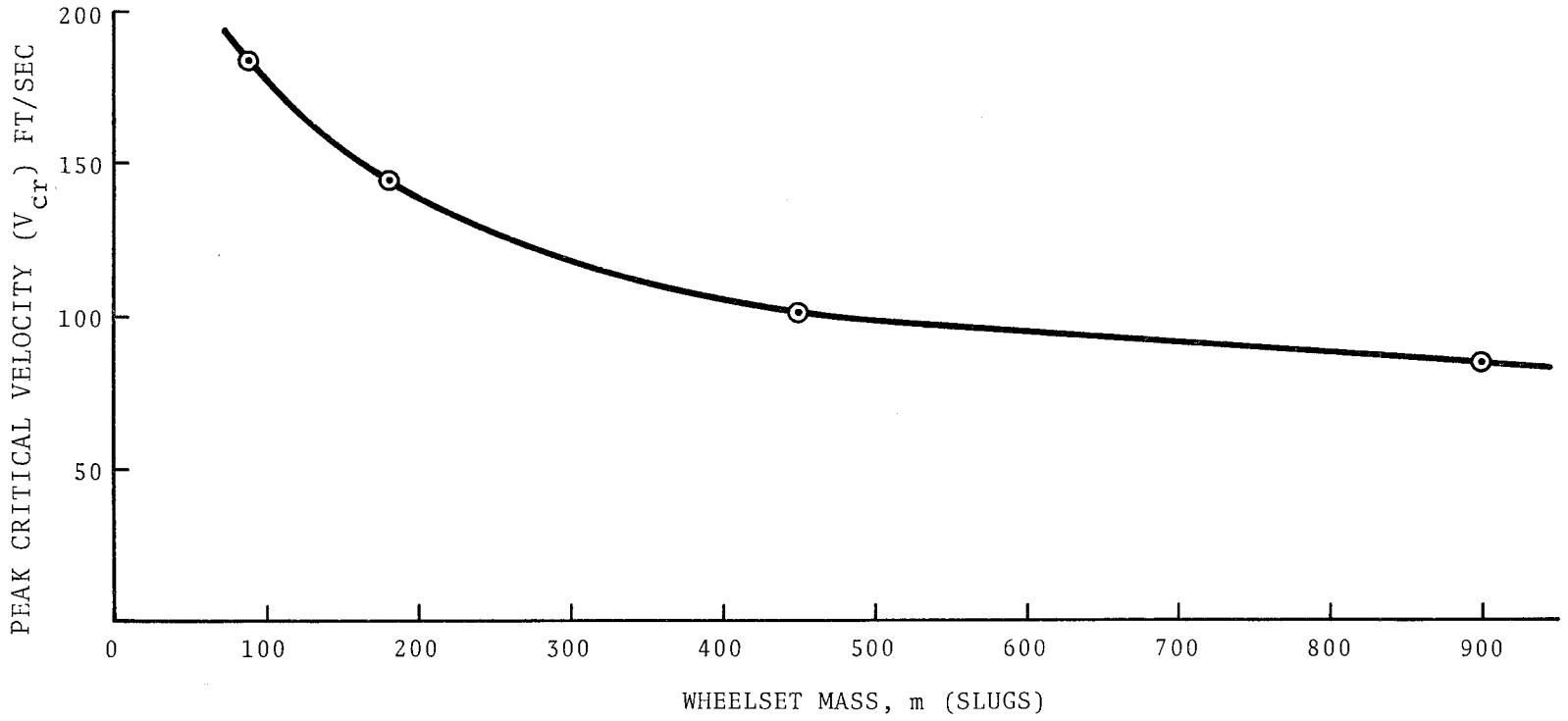

Figure 6-7. Effect of Variation in Wheelset Mass on the Peak Critical Velocity with a Constant Creep Coefficient of 4×10^5 lb

The describing function of effective conicity α_e^*, for the conical profile of a new wheel as a function of lateral oscillation amplitude is shown in Figure 6-8. For a straight tapered cone profile it is a constant equal to the cone angle of the tread. This is obvious from Figure 6-8 for the conical portion of the wheel. The value of the taper over the linear range is 1 in 20. However, for the nonlinear range the effective conicity is derived from the difference in rolling radii as the wheelset is displaced laterally from its nominal position. The describing function α_e^* is a function of the lateral oscillation amplitude for the wheelset as shown in the figure.

Figure 6-9 shows K_g^*, the describing function of the gravitational stiffness for a new wheel with conical profile. The gravitational stiffness arises due to an elevation of the center of gravity as the wheelset is displaced laterally. Again, it is dependent on the difference in rolling radii between opposite wheels, which in turn is a function of the amplitude of lateral oscillations. The describing function for gravitational stiffness is essentially zero for the linear portion of the wheel, rises over the flange portion of the wheel and finally decreases as the flange profile starts to level off.

The gravitational Force, F_g, as a function of the amplitude of lateral oscillations, is shown in Figure 6-10. The plot is similar in trend to the plot of gravitational stiffness describing function illustrated in the previous figure. As before, the gravitational force is nearly zero for approximately 0.075 ft (0.9 inch) from the centered position. The gravitational force increases over the flange

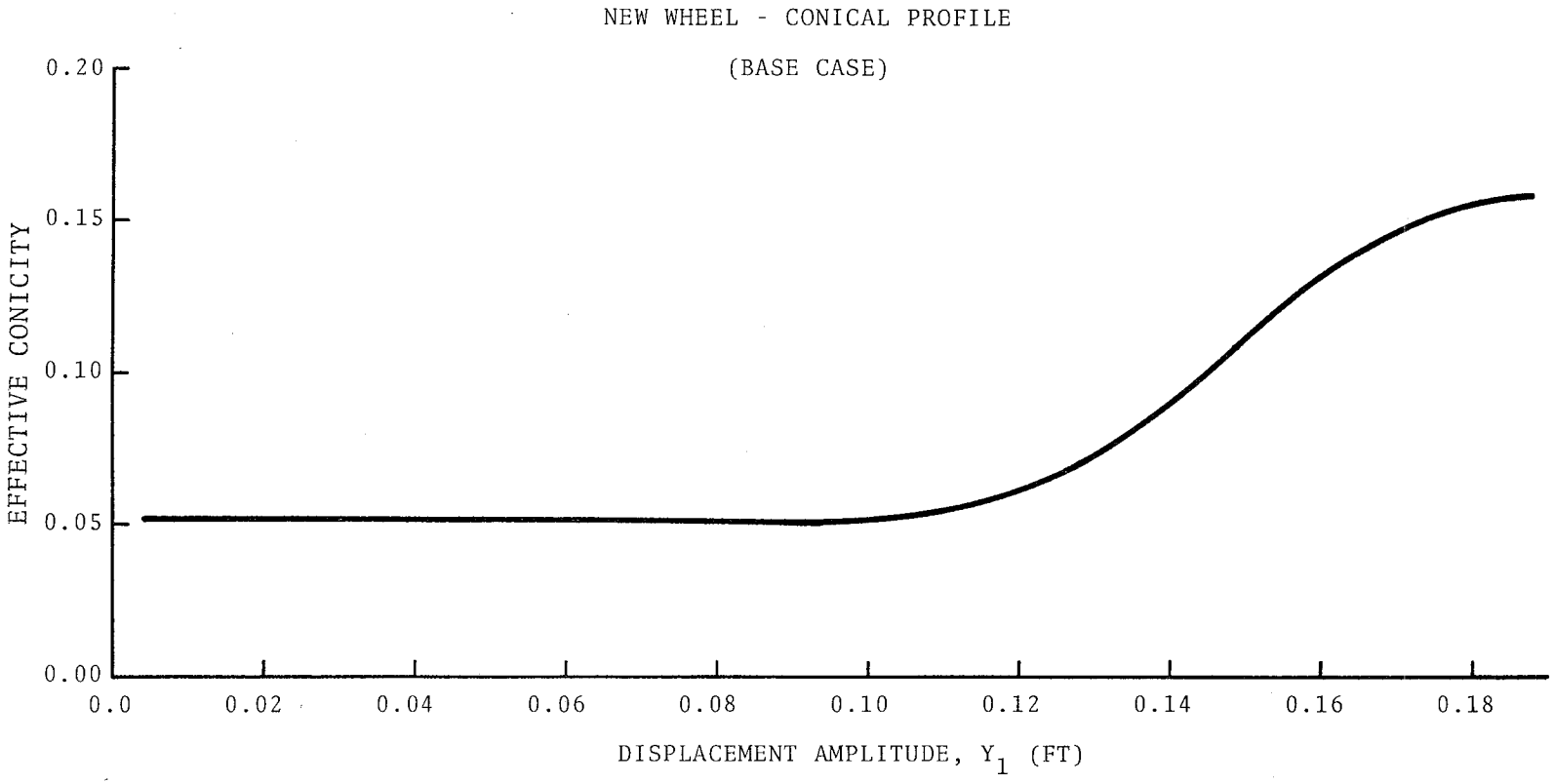

Figure 6-8. A Plot for Describing Function of Effective Conicity as a Function of Amplitude of Wheelset Oscillations

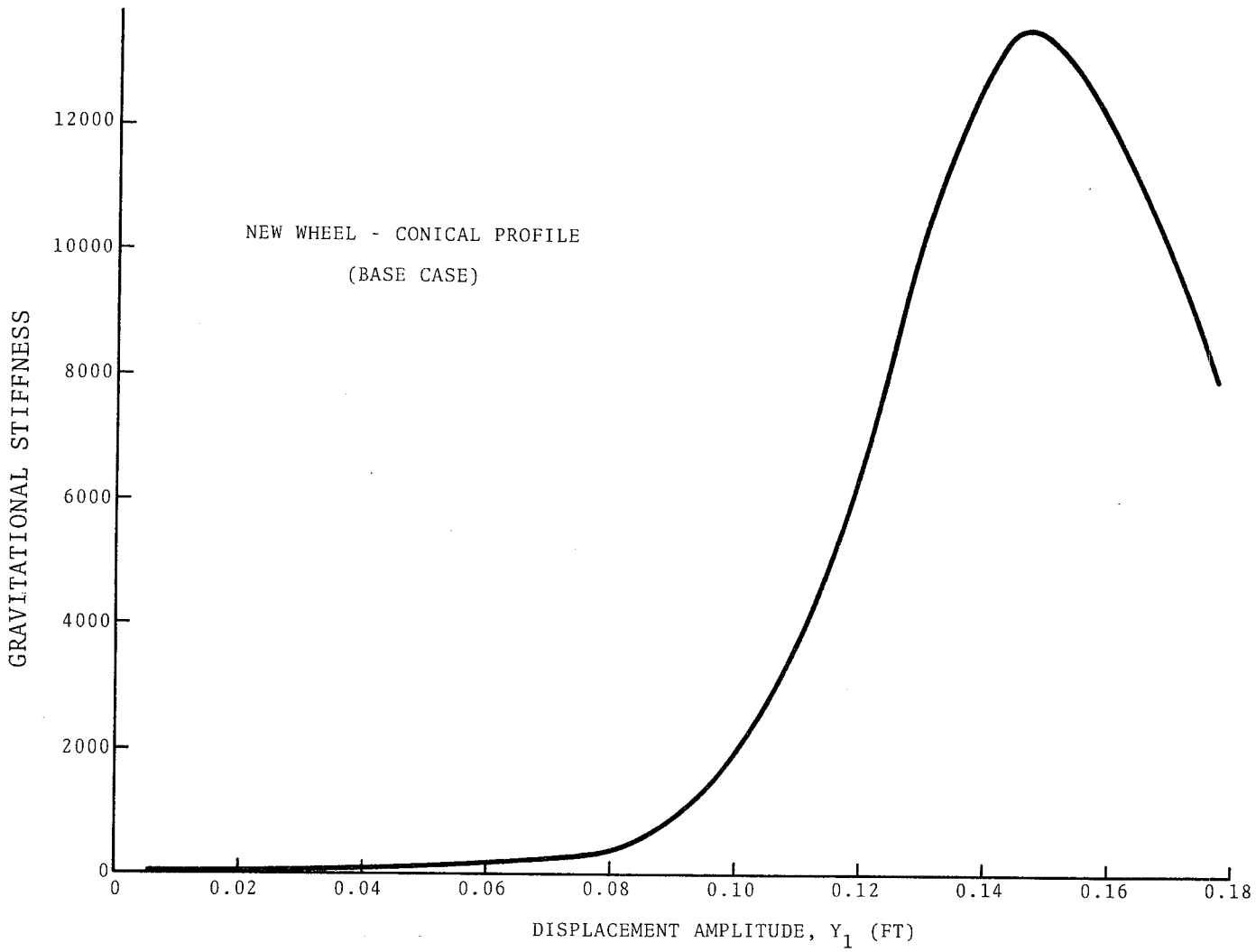

Figure 6-9. K_g*, the Describing Function of Gravitational Stiffness, Plotted as a Function of Lateral Amplitude of Wheelset Oscillations

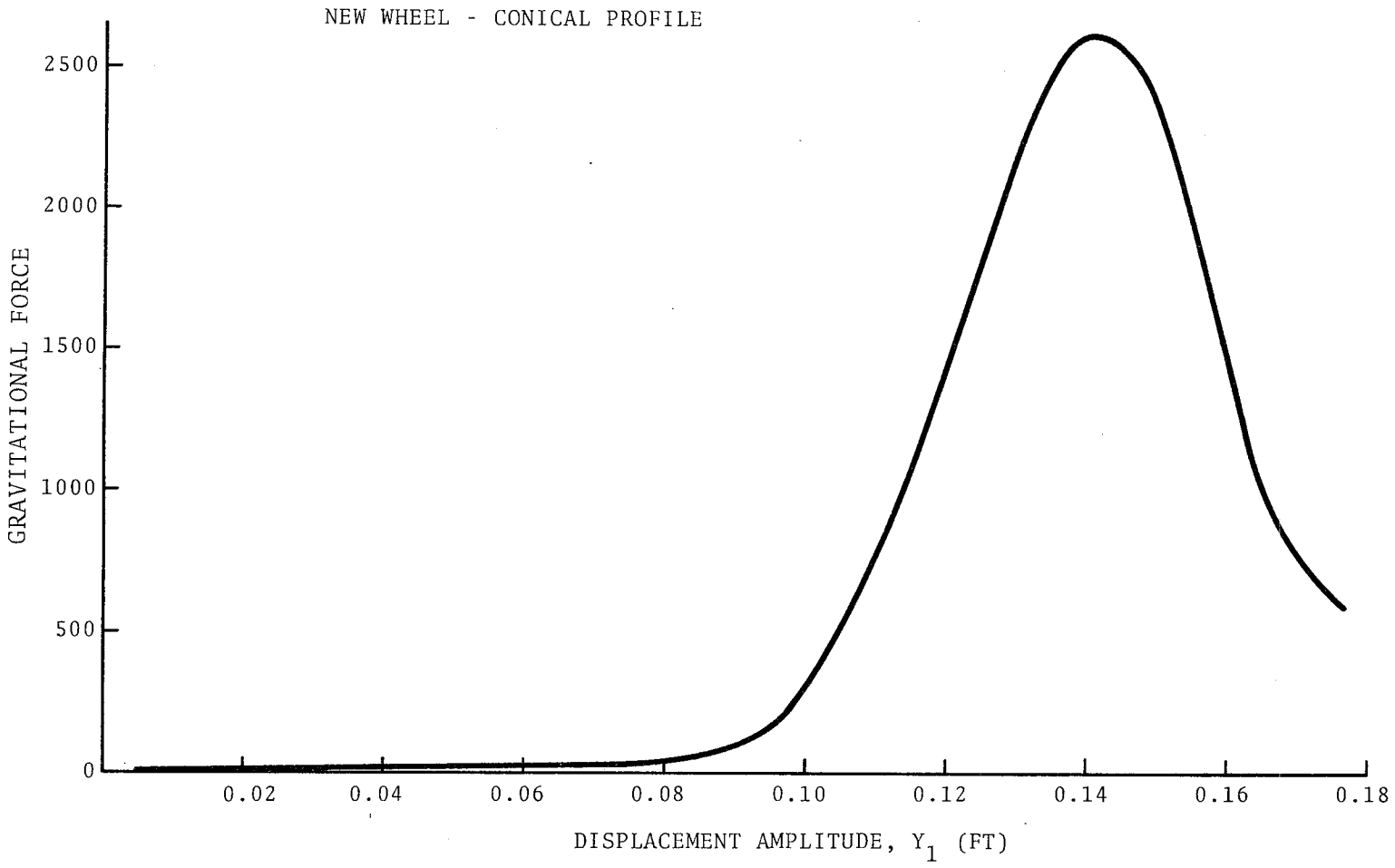

Figure 6-10. Plot of Gravitational Force as a Function of Amplitude of the Lateral Oscillations

portion of the profile and subsequently decreases after reaching a maximum at about 0.14ft (1.68 inch) from the mean position.

Figure 6-11 shows a plot of yaw displacement, ψ, as a function of the amplitude of lateral oscillations. Since the critical speed is also a function of the amplitude of lateral oscillation (Figure 6-1) this plot may also be redrawn in terms of V_{cr} versus ψ values. Such a plot may help to interpret the relationship between hunting and rotational amplitude of the wheelset oscillation. The value of ψ is computed from the frequency-dependent relationship.

$$|\psi| = \frac{\sqrt{[(K_g^* + k_y) - m\omega^2]^2 + (\frac{2f_L\omega}{V})^2}}{2f_L} |Y_1(j\omega)|$$

Alternatively, the value of ψ may be obtained using the relationship:

$$|\psi| = \frac{2f_T\ell(\alpha_e^*/r_o)}{\sqrt{[(k_\psi - K_a^*) - C\omega^2]^2 + (\frac{2f_T\ell^2\omega}{V})^2}} |Y_1(j\omega)|$$

These expressions are based upon the nonlinear equations describing the dynamical behavior of the wheelset. In both of the expressions, the right hand side terms are known for each assumed value of Y_1.

Under the assumption of linear creep, the lateral and longitudnal components of creep velocity were computed using the following relationships. The magnitude of the lateral component is given by:

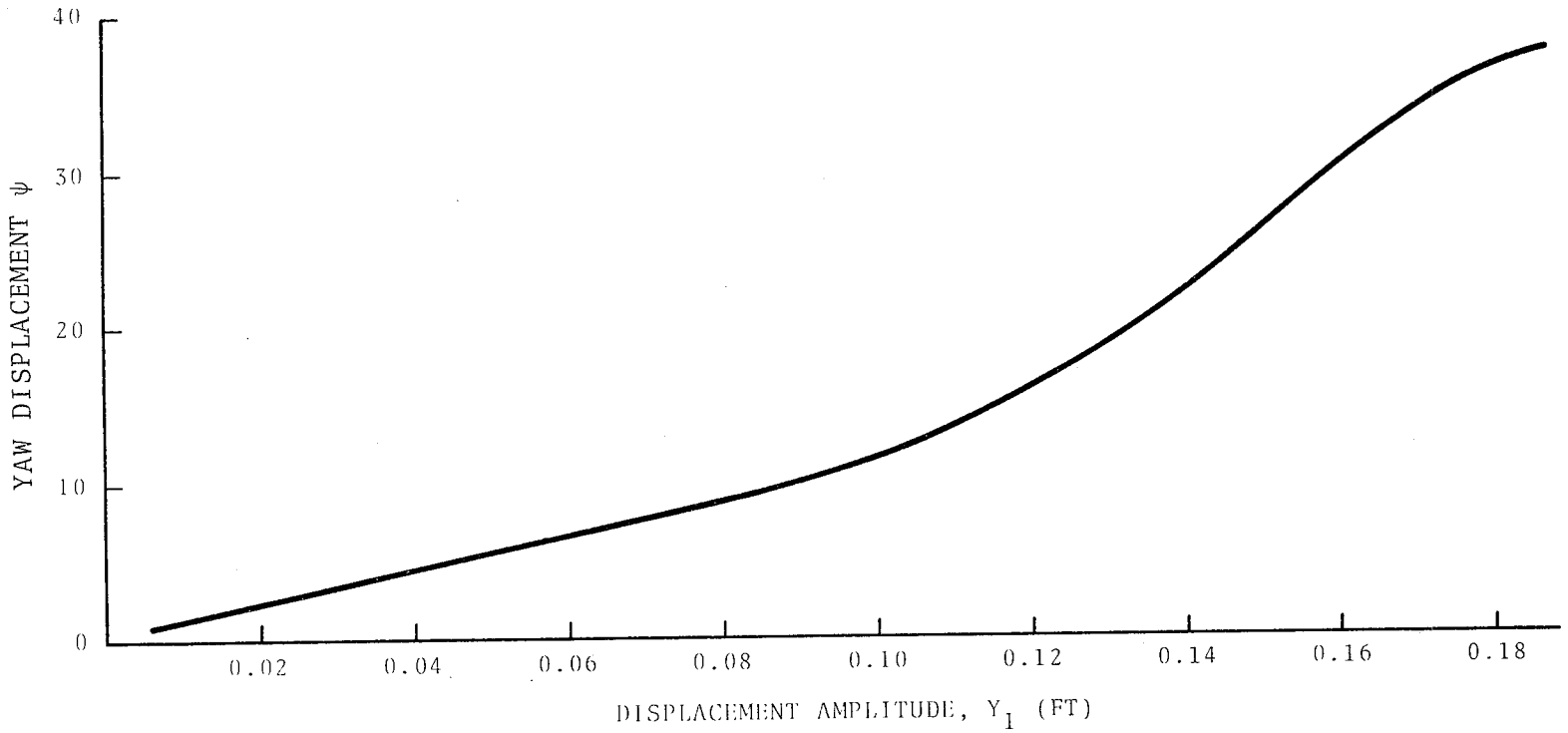

Figure 6-11. Plot of Yaw Displacement Ψ as a Function of the Amplitude of Lateral Oscillations

$$|\xi_L| = \sqrt{(\frac{\omega}{V})^2 (Y_1)^2 + \psi^2}$$

and the same for the longitudinal (forward) component is given by:

$$|\xi_T| = \sqrt{(\frac{\alpha_e}{r_o})^2 (Y_1)^2 + (\frac{\ell\omega}{V})^2 \psi^2} .$$

The plots of ξ_L and ξ_T, the lateral and forward components of creep velocity or creepage are shown in Figure 6-12. The forward or transverse component is no more than 50% of the lateral component over the entire range of Y_1 values. The corresponding creep forces can be obtained, straightforwardly, as the product of creepage and creep coefficients. The significance of the creep forces is the following:

As the wheelset speed increases in the forward direction, the creep forces generated at the wheel treads also increase until their vector sum equals the limiting friction between wheel and rail. Slipping starts at this stage, and yaw and lateral oscillations attain their maximum levels.

The foregoing plots and discussion illustrate the dynamic behavior of the wheelset and the effect of variation in various parameters on the amplitude and frequency of hunting motion in the lateral mode. The describing function method of analysis was used. The information is helpful in dynamic analysis, modeling, and parametric study of rail systems.

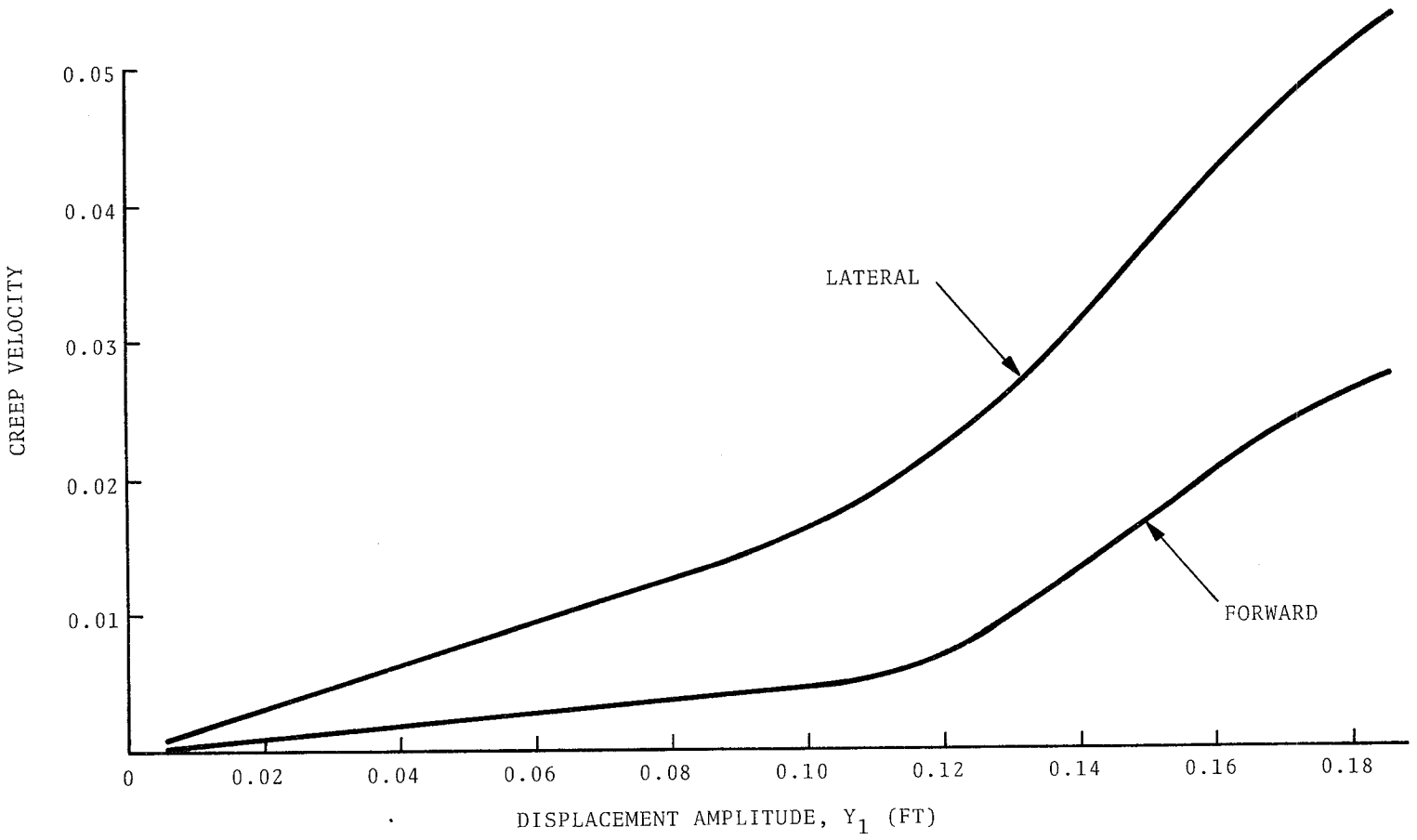

Figure 6-12. Lateral and Transverse Creep Velocity Components as a Function of the Amplitude of Lateral Oscillations

7. CONCLUSIONS

Sustained oscillation of wheelsets traveling over rails cause serious problems leading to an unsatisfactory operation of entire vehicle. The wheels are subjected to forces while negotiating curves [B1, K3], or forces arising from the rail irregularities [L4,S1,S2]. Several analytical studies have been undertaken in the past to model the rail-wheel interaction and develop a better understanding of the complex dynamic phenomenon. Many investigations have been restricted to linear analyses, however, thus restricting their validity to small deviations from the equilibrium state.

In actual operation, large scale excursions from the operating point are quite common and as such require new and convenient tools to predict the dynamical behavior applicable over a broader range of operation. The phenomenon of hunting at high speeds is fairly well-known. In addition to providing poor ride characteristics, hunting has been responsible for derailments of wheelsets and bogies.

This report has dealt with the secondary hunting problem associated with a wheelset consisting of a pair of wheels connected via a rigid axle. The wheels are assumed to have a nonlinear profile, either in the new or in the worn state. The analytical expression for a given profile is in a polynomial form, and the coefficients of the polynomial are obtained using a least-square curve fit algorithm. Linear lateral and transverse creep coefficients are assumed.

A describing function based approach is developed to arrive at the critical velocity and amplitude of lateral oscillations relationship. Influence of change in parameters on critical velocity is also examined using the same approach. The method is tested by applying it to a system published in literature and analysed by the Krylov and Bogoliubov method. The proposed approach yields comparable results, and has the added advantage of being general and equally applicable to systems of higher order and complexity.

The method was applied to three types of profiles: a conventional conical profile (described by an eighteenth-degree polynomial), a tread-worn conical profile (described by a seventeenth-degree polynomial), and a cylindrical profile (described by a sixteenth-degree polynomial).

The following conclusions were obtained from the results obtained in this report:

1. While tread wear has an influence on the peak value of critical velocity, the general shape of the response curve is similar to that in the case of new wheel.

2. An increase in axle load increases the value of peak critical velocity and hence has a stabilizing effect.

3. An increase in each, the lateral and yaw stiffness, leads to an increase in the value of critical velocity and hence has a beneficial effect on high speed operational stability of the wheelset.

4. The influence of change in wheelset mass on peak critical velocity is rather small. An increase in wheelset mass causes a decrease in peak critical velocity.

In addition to the specific conclusions enumerated above it may be remarked that whereas the proposed technique of representing a profile by a polynomial is basically appropriate, the results are sensitive to the polynomial coefficients. An alternate description of the profile may be via a combination of straight lines and arcs of circles. Further work needs to be done in the area of an accurate and convenient representation of the wheel profile.

The research outlined in the present report considered an ideal knife-edged rail. A more realistic analysis will have to take into account the rail head profile and its changes with a wear in the wheel profile.

The effect of including nonlinear creep forces in the analysis may be examined. The present report considers only constant creep coefficients, thus limiting creep forces below their limiting value of coulomb friction. Further analysis should explore this aspect of the problem.

REFERENCES

A1 Atherthon, D., Turnbull, G., Gello, A., and Vander Velde, W.: Discussion of the Double Input Describing Function (DIDF) for Unrelated Sinusoidal Signals, IEEE Transactions on Automatic Control, Vol AC-9, No. 2, April 1964, pp. 197-198.

A2 Axelby, G.: Random Noise with Bias Signals in Nonlinear Devices, IRE Transactions on Automatic Control, Vol.AC-4, No. 2, November 1959, pp. 167-181.

B1 Boocock, D.: Steady-State Motion of Railway Vehicles on Curved Track, Journal of Mechanical Engineering Science, Vol. 11, No. 6, 1969, pp.556-566.

B2 Blader, F., and Kurtz, E.: Dynamic Stability of Cars in Long Freight Trains, ASME Paper No. 73-WA/RT-2, 1973.

B3 Bennington, C.: The Railway Wheelset and Suspension Unit as a Closed-Loop Guidance Control System: A Method for Performance Improvement, Journal of Mechanical Engineering Science, Vol. 10, No. 2, 1968, pp. 91-100.

B4 Bogoliubov, N.N. and Mitropolski, J.A.: Asymptotic Methods in the Theory of Nonlinear Oscillations, State Press for Physics and Mathematical Literature, Moscow, 1963.

B5 Brann, R.: Some Aspects of the Hunting of a Railway Axle, Journal of Sound and Vibration, Vol 4, No. 1, 1966, pp. 18-32.

C1 Cooperider, N.: The Hunting Behavior of Conventional Railway Trucks, Journal of Engineering for Industry, Transactions of the ASME, Vol. 94, No. 2, May 1972, pp. 752-762.

C2 Clark, J. and Law, E.: Investigation of the Truck Hunting Instability Problem of High-Speed Trains, ASME Paper No. 67-TRAN-17, 1967.

C3 Cooperider, N.: High Speed Dynamics of Conventional Railway Trucks, Ph.D. Thesis, Stanford University, 1968.

D1 Davies, R.: Some Experiments on the Lateral Oscillation of Railway Vehicles, Journal of the Institute of Civil Engineers, Vol. 11, 1930, pp. 224-261.

D2 De Pater, A.: The Approximate Determination of the Hunting Movement of a Railway Vehicle by aid of the Method of Krylov and Bogoliubov, Applied Scientific Research, Section A, Vol.10, 1961, pp. 205-228.

G1 Gelb, A. and Vander Velde, W.: Multiple-Input Describing Functions and Nonlinear System Design, McGraw-Hill, New York, 1968.

G2 Gilchrist, A.O., et al: The Riding of Two Particular Designs of Four-Wheeled Railway Vehicle, Proceedings of the Institution of Engineers, Vol. 180, Pt. 3F, 1966, pp. 99-113.

J1 Johnson, K.: The Effect of Spin Upon the Rolling Motion of an Elastic Sphere on a Plane, Journal of Applied Mechanics, Transactions of the ASME, Vol. 80, Sept. 1958, pp. 332-338.

J2 Johnson, K.: The Effect of a Tangential Contact Force Upon the Rolling Motion of an Elastic Sphere on a Plane, Journal of Applied Mechanics, Transactions of the ASME, Vol. 80, Sept. 1958, pp. 339-346.

K1 King, B.: Tyre Profiles, Paper No. 14, Presented at the Third International Wheelset Conference, Sheffield, July 1969.

K2 Kochenburger, R.: A Frequency Response Method for Analyzing and Synthesizing Contactor Servomechanisms, AIEE Transactions Pt. I (Power Apparatus and Systems), Vol. 69, 1950, pp.270-284

K3 Koci, L. and Marta, H.: Lateral Loading Between Locomotive Truck Wheels and Rail Due to Curve Negotiation, ASME Paper No. 65-WA/RR-4, 1965.

L1 Law, E.: Analysis of the Nonlinear Dynamics of a Railway Vehicle Wheelset, Ph.D. Thesis , University of Connecticut, 1971.

L2 Law, E., and Brand, R.: Analysis of the Nonlinear Dynamics of a Railway Vehicle Wheelset, Journal of Dynamic Systems, Measurement, and Control, Transactions of the ASME, Vol. 95, No. 1, March 1973, pp. 28-35.

L3 Law, E. and Cooperrider, N.: A Survey of Railway Vehicle Dynamics Research, Journal of Dynamic Systems, Measurement, and Control, Transactions of the ASME, Vol 96, No. 2, June, 1974, pp. 132-146.

L4 Law, E.: Nonlinear Wheelset Dynamic Response to Random Lateral Rail Irregularities, ASME Paper No. 73-WA/RT-3, 1973.

M1 Matsudaira, T.: Hunting Problems of High-Speed Railway Vehicles with Special Reference to Bogie Design for the New Tokaido Line, Proceedings of the Institution of Engineers, Vol. 180. Pt. 3F, 1966, pp. 58-66.

M2 Matsudaira, T. et.al.: Problems on Hunting of Railway Vehicle on Test Stand, Journal of Engineering for Industry, Transactions of the ASME, Vol. 91, No. 3, August 1969, pp. 879-890.

M3 Meacham, H. and Ahlbeck, D.: A Computer Study of Dynamic Loads Caused by Vehicle-Track Interaction, Journal of Engineering for Industry, Transactions of the ASME, Vol. 91, No. 3, August 1969, pp. 808-816.

M4 Marcotte, P.: Lateral Dunamic Stability of Railway Bogie Vehicles, M.S. Thesis, University of Sheffield, May 1972.

M5 Minorsky, N.: Theory of Nonlinear Control Systems, McGraw-Hill, New York, 1969.

O1 Oldenburger, R. and Boyer, R.C.: Effects of Extra Sinusoidal Inputs to Nonlinear Systems, Transactions of the ASME, Series D, Journal of Basic Engineering, Vol. 84, No. 4, December 1962, pp. 559-570.

R1 Reynolds, D.: Hunting in Freight Cars, ASME Paper No. 74-RT-2, 1974.

S1 Siddall, J., Dokainish, M. and Elmarghy, W.: On the Effect of Track Irregularities on the Dynamic Response of Railway Vehicles, ASME Paper No. 73-WA/RT-1, 1973.

S2 Stassen, H.: Random Lateral Motions of Railway Vehicles, Doctoral Thesis, Delft Technological University, 1967.

V1 Vander Vegte, J. and Royle, R.: Triple Input Describing Functions and the Stability Analysis of Forced Nonlinear Control Systems, JACC Preprints, 1967, pp. 499-504.

V2 Vermeulen, P., and Johnson, K.: Contact of Nonspherical Elastic Bodies Transmitting Tangential Forces, Journal of Applied Mechanics, Transactions of the ASME, Vol. 86, No. 2, June 1964, pp. 338-340.

W1 Weinstock, H.: Analyses of Rail Vehicle Dynamics in Support of Development of the Wheel Rail Dynamics Research Facility, Report No. MA-06-0025-73, TSC, Cambridge, Mass., 1973.

W2 Wickens, A.: The Dynamics of Railway Vehicles on Straight Track: Fundamental Considerations of Lateral Stability, Proceedings of the Institution of Mechanical Engineers, Vol. 180, Part 3F, 1966, pp. 29-44.

W3 Wickens, A.: The Dynamic Stability of Railway Vehicle Wheelsets and Bogies Having Profiled Wheels, International Journal of Solids and Structures, Vol. 1, No. 3, 1965, pp. 319-341.

W4 Wickens, A.: General Aspects of the Lateral Dynamics of Railway Vehicles, Journal of Engineering for Industry, Transactions of the ASME, Vol. 91, No. 3, August 1969, pp.869-878.

APPENDIX A

PROFILES USED

AND

COMPUTER PLOTS

Appendix A presents the graphic displays of profiles used, computer generated coefficients and plots for a least-square polynomial fit obtained using the FORTRAN program FITIT (developed for DEC-10 System available at TSC), and the plots of difference in rolling radii of two opposite wheels of the wheelset as a function of lateral displacement. For example, Figure A-1 is a plot of the conical wheel profile. The vertical bars and the numbers represent the discrete data used as input to the polynomial fit program. The data was fed in feet units and Figure A-2 shows the values of coefficients a_o, a_1, . . . , a_{18} of the 18th-degree polynomial used for fitting the polynomial through the set of discrete data points. The points marked X represent the input data from Figure A-1. As is evident from Figure A-2, an 18th-degree polynomial provides a satisfactory fit to the conical profile. Figure A-3 is a plot of differences in rolling radii for the conical profile as a function of lateral displacement. The curve is negative symmetric, as one would expect, and is useful in computing the effective conicity of the profile.

Figures A-4,A-5 and A-6 present the above profile in the case of a conical wheel. The details of the wear pattern are evident from Figure A-4.The computer generated plot and the coefficient of the least-square fit polynomial are shown in Figure A-5. A seventeenth-degree polynomial provided a good fit in this case. Figure A-6 is the plot of difference in rolling radii versus lateral displacement.

Figures A-7,A-8 and A-9 contain the set of plots for a new cylindrical wheel. In this case a sixteenth-order polynomial adequately represented the profile. The values of coefficients for input data in feet are also shown in Figure A-8.

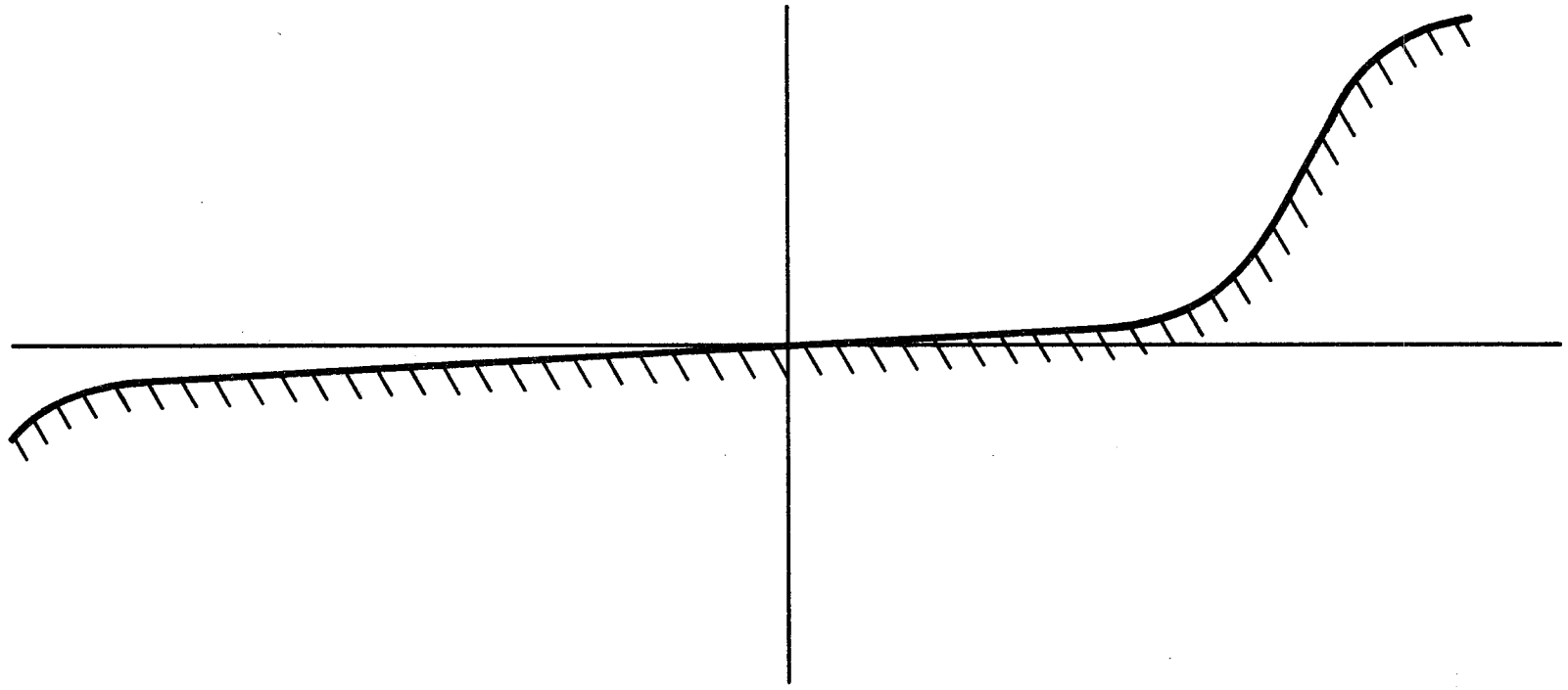

Figure A-1. Tire Profile for a New Wheel with a Conical Profile

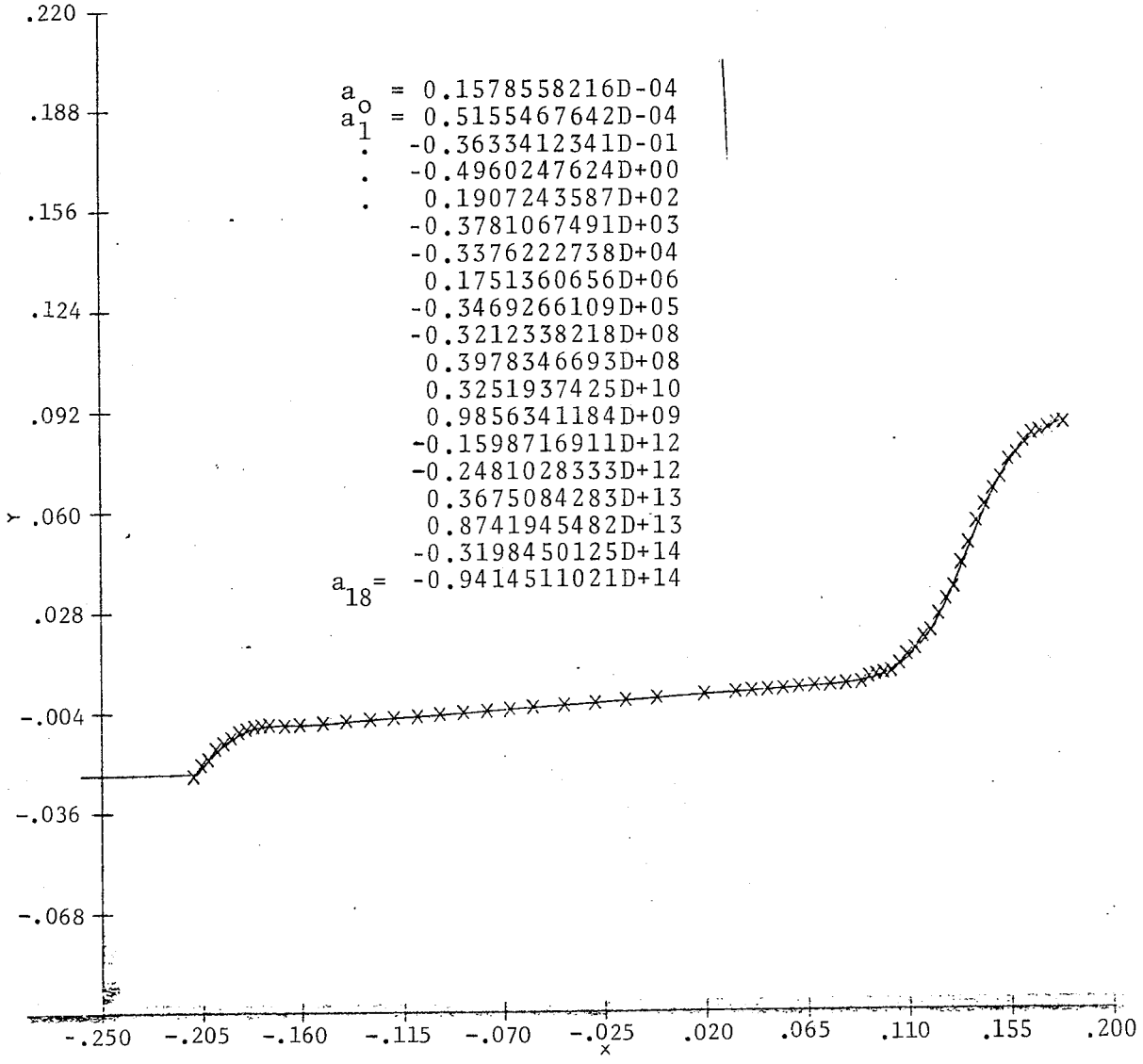

Figure A-2. Least-Square Fit Polynomial Coefficients Input Data Points and Computer Generated Profile for the Conical Tire

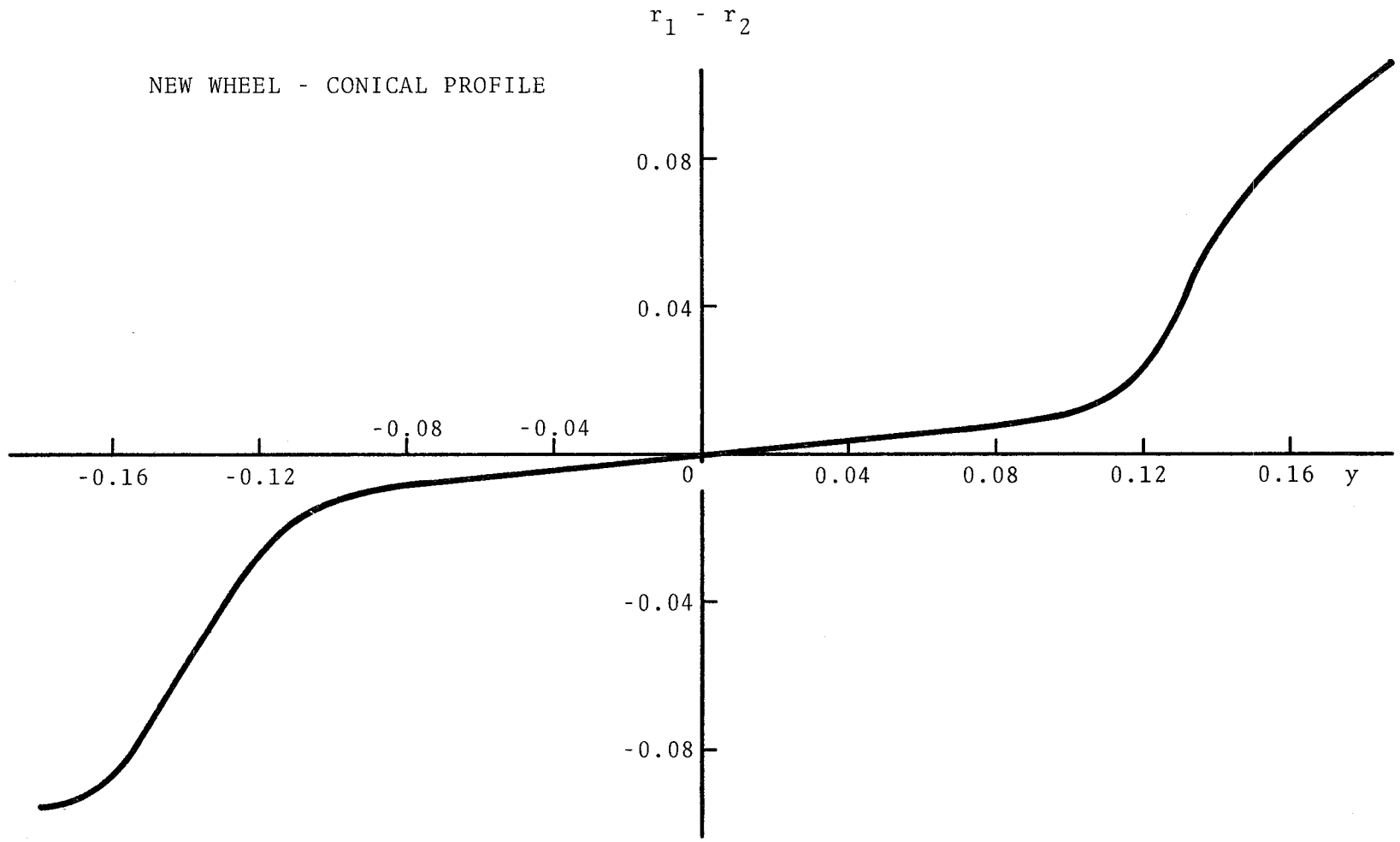

Figure A-3. Difference in Rolling Radii of Opposite Wheels Plotted as a Function of Lateral Displacement

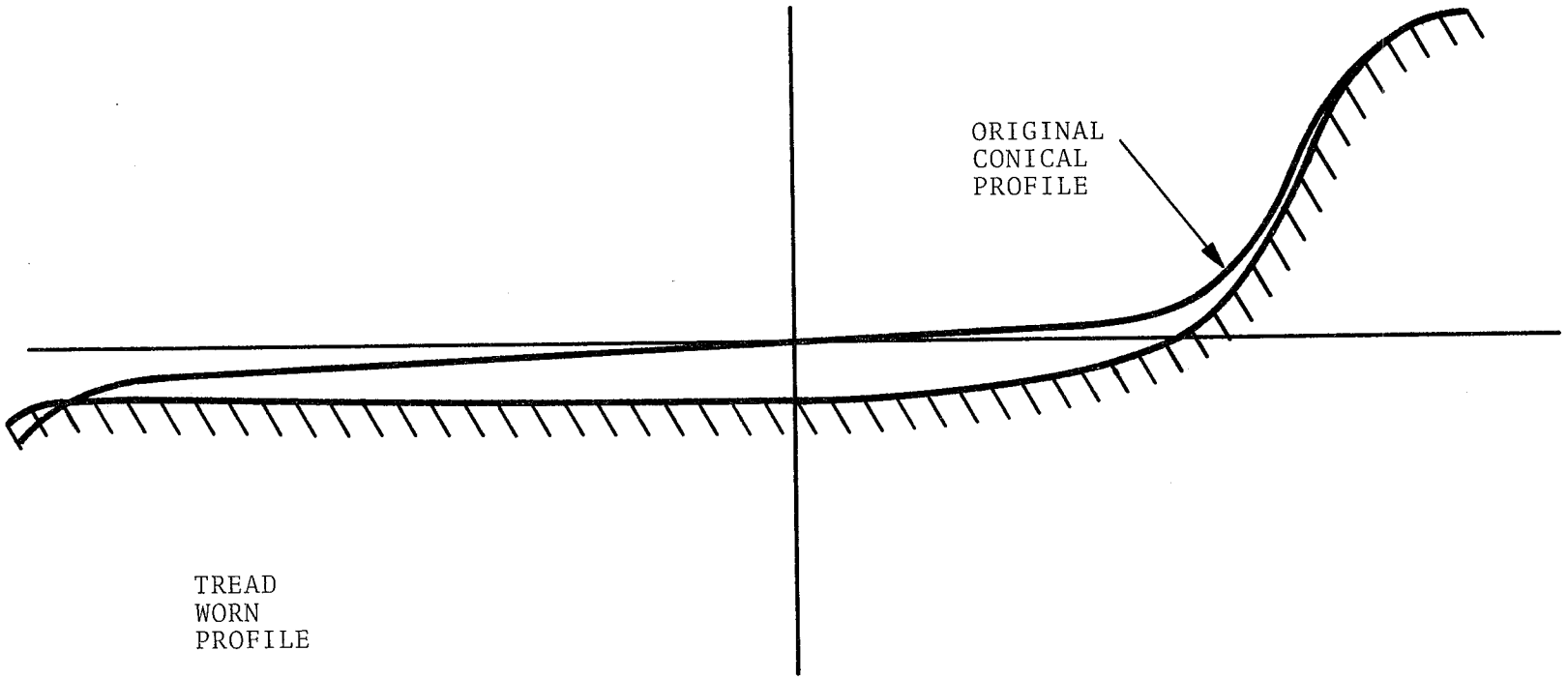

Figure A-4. Original Conical and Tread-Worn Profiles Used for Analysis. Note that Most of the Wear is on the Tread

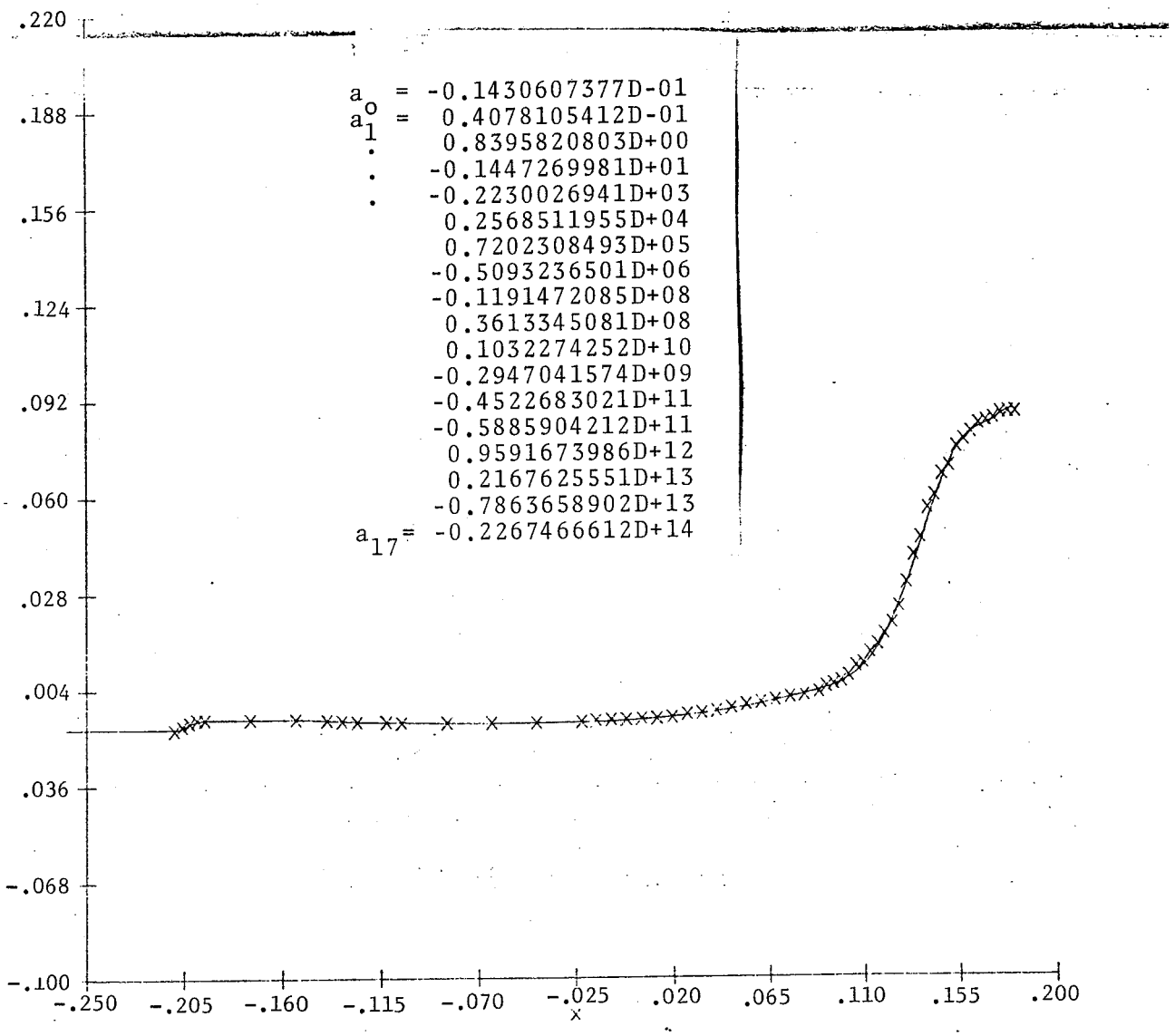

Figure A-5. Least-Square Fit Polynomial Coefficients, Input Data Points (Ft) and Computer Generated Plot for the Tread-Worn Conical Wheel Profile

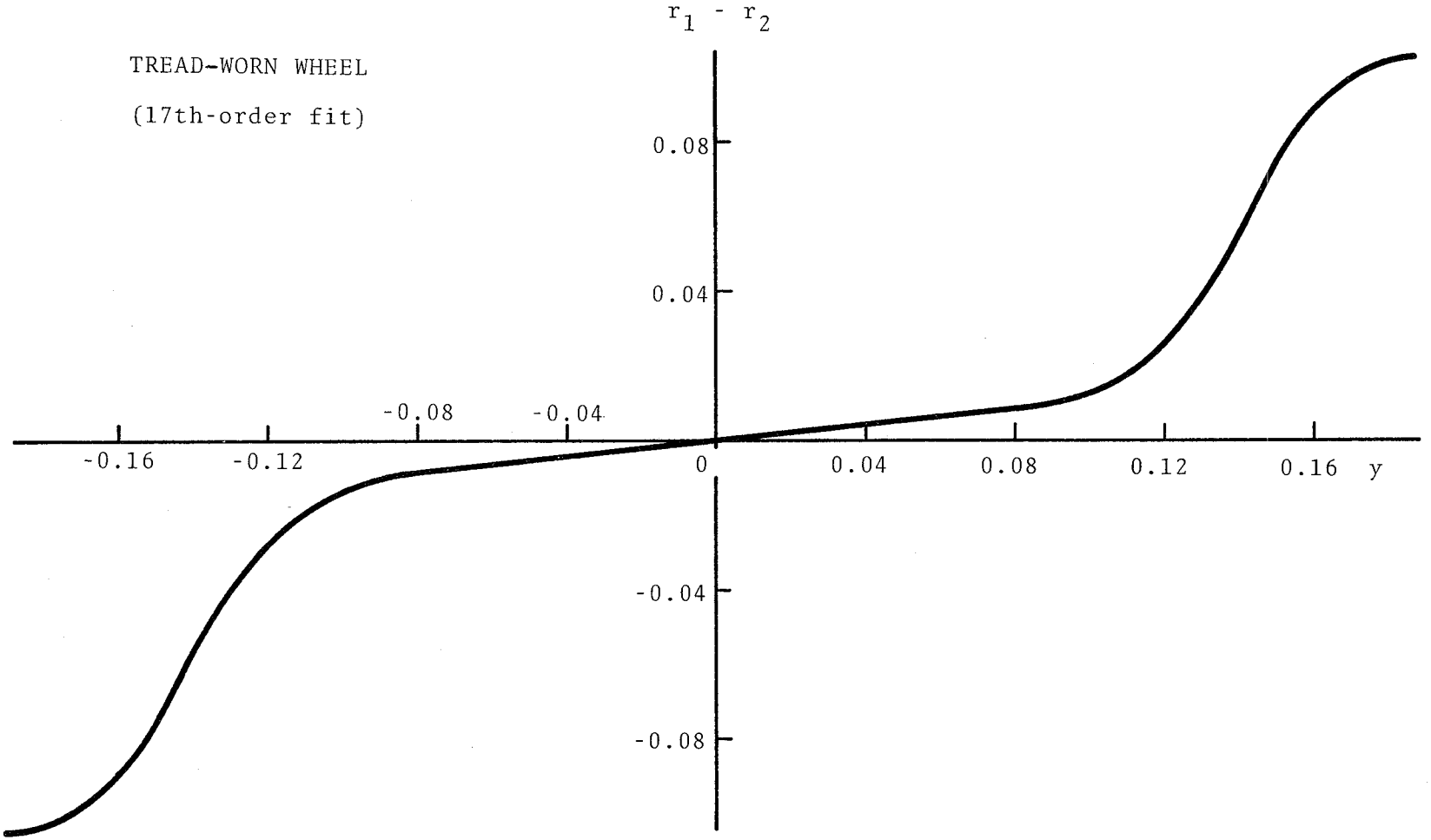

Figure A-6. Difference in Rolling Radii of the Opposite Wheels of the Wheelset Vs. Lateral Displacement for the Tread-Worn Case

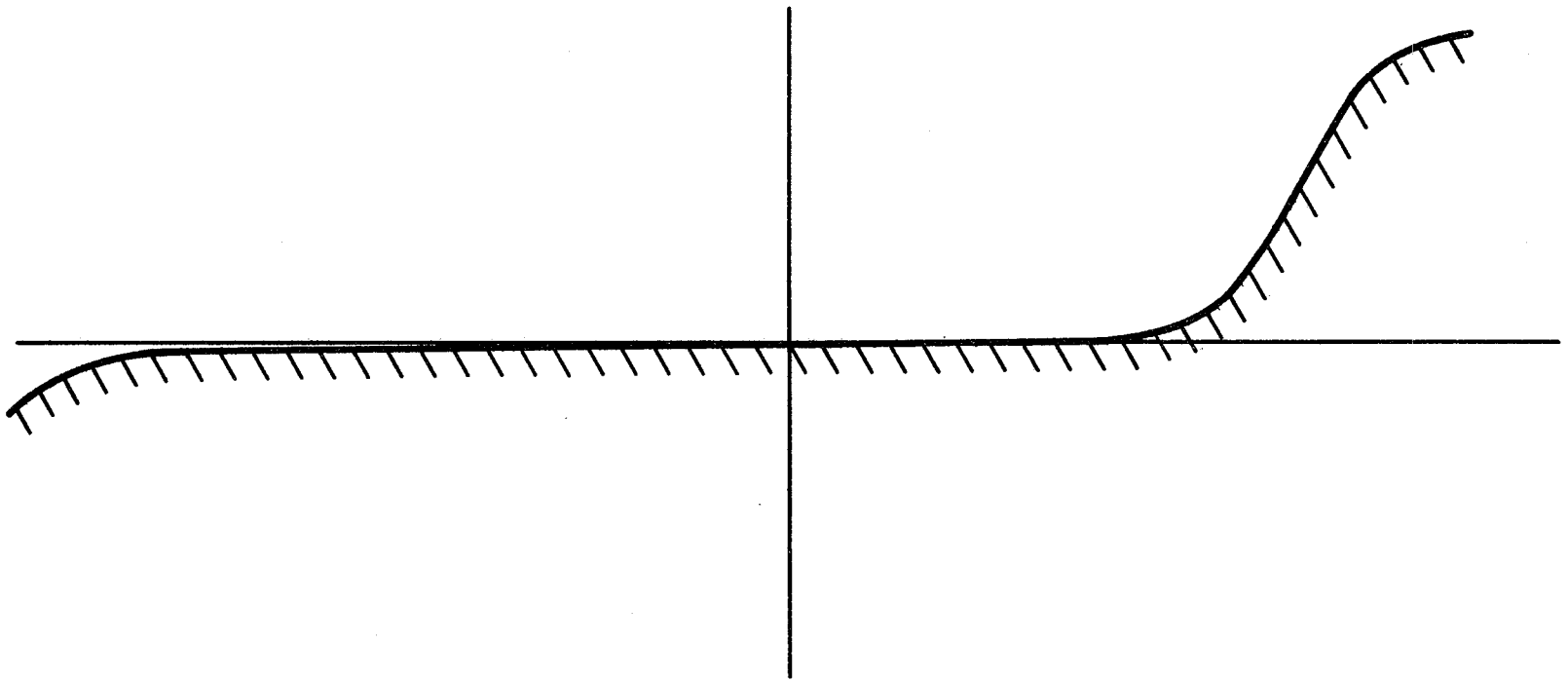

Figure A-7. Basic Profile of a Wheel Tire with a Cylindrical Profile

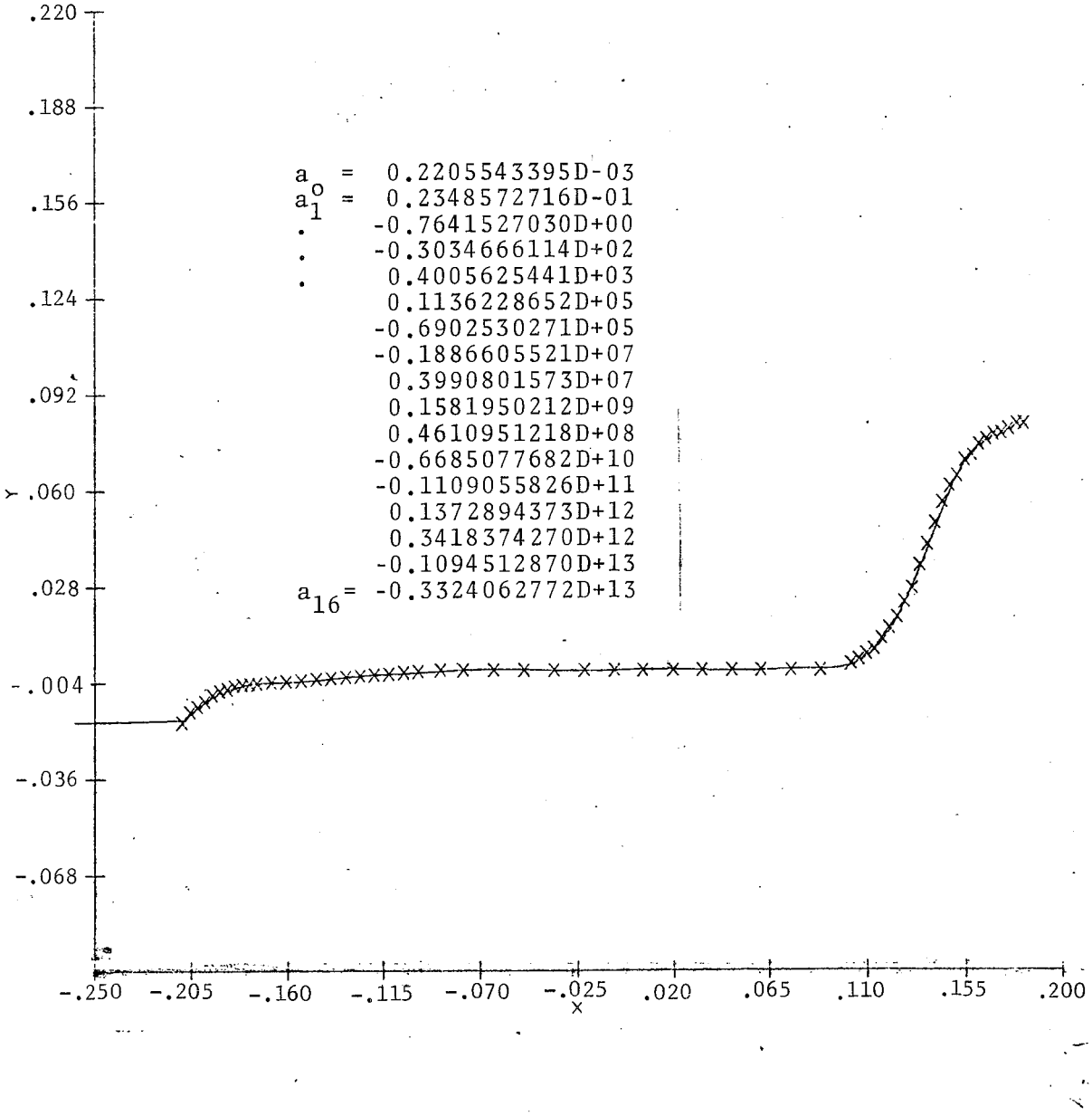

Figure A-8. Least-Square Polynomial Fit Coefficients, Input Data Points (Ft) and Computer Generated Plot for the Tire Profile. A Sixteenth-order Polynomial Yielded a Good Fit

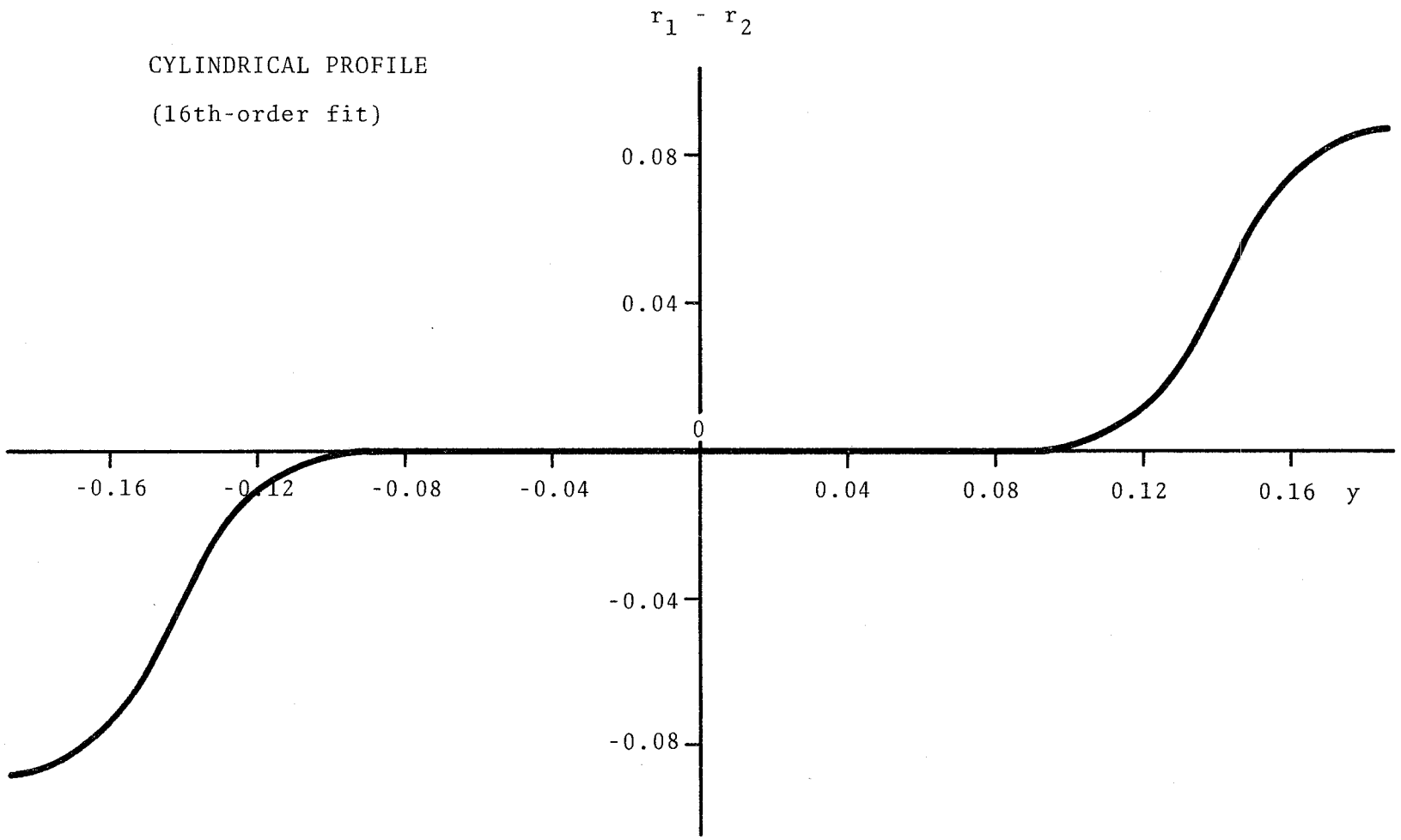

Figure A-9. Difference in Rolling Radii Vs. Lateral Displacement for the Case of Cylindrical Profile

APPENDIX B

COMPUTER PROGRAM LISTING

FOR EXAMPLE SYSTEM

Law and Brand [L2] have formulated an analytical model for nonlinear dynamics of a vehicle wheelset traveling on straight tracks. The wheel profile in the model was assumed to be nonlinear, creep forces and moments to be linear, and a rail-wheel contact force to consist of a deadband and linear spring characteristic. The Krylov and Bogoliubov method of analysis was used in Reference L2.

A dynamic model in terms of nonlinear differential equations was set up to evaluate the amplitude of stationary oscillations. Stability conditions were derived using a perturbation analysis. It was shown that the flange clearance and the nonlinear variation of axle roll with lateral displacement had a significant influence on the motion of the wheelset. The results were graphically presented to portray the effect of wheel profile curvature parameter and non-dimensional flange clearance on the oscillation amplitude.

For the purposes of this report, the describing function approach outlined at the end of Section 4 was applied to the system used in Reference L2. The describing function for deadband type nonlinearity was derived. The equivalence between the model presented in Reference L2 and the one proposed in the present report was established and the values of equivalent parameters were identified. Based on these parameteric values, Figure B-1 was obtained using the proposed approach. The dimensional values obtained as well as the corresponding nondimensional parameters (such as used in Figure 7 of Reference L2) are labeled in Figure B-1.

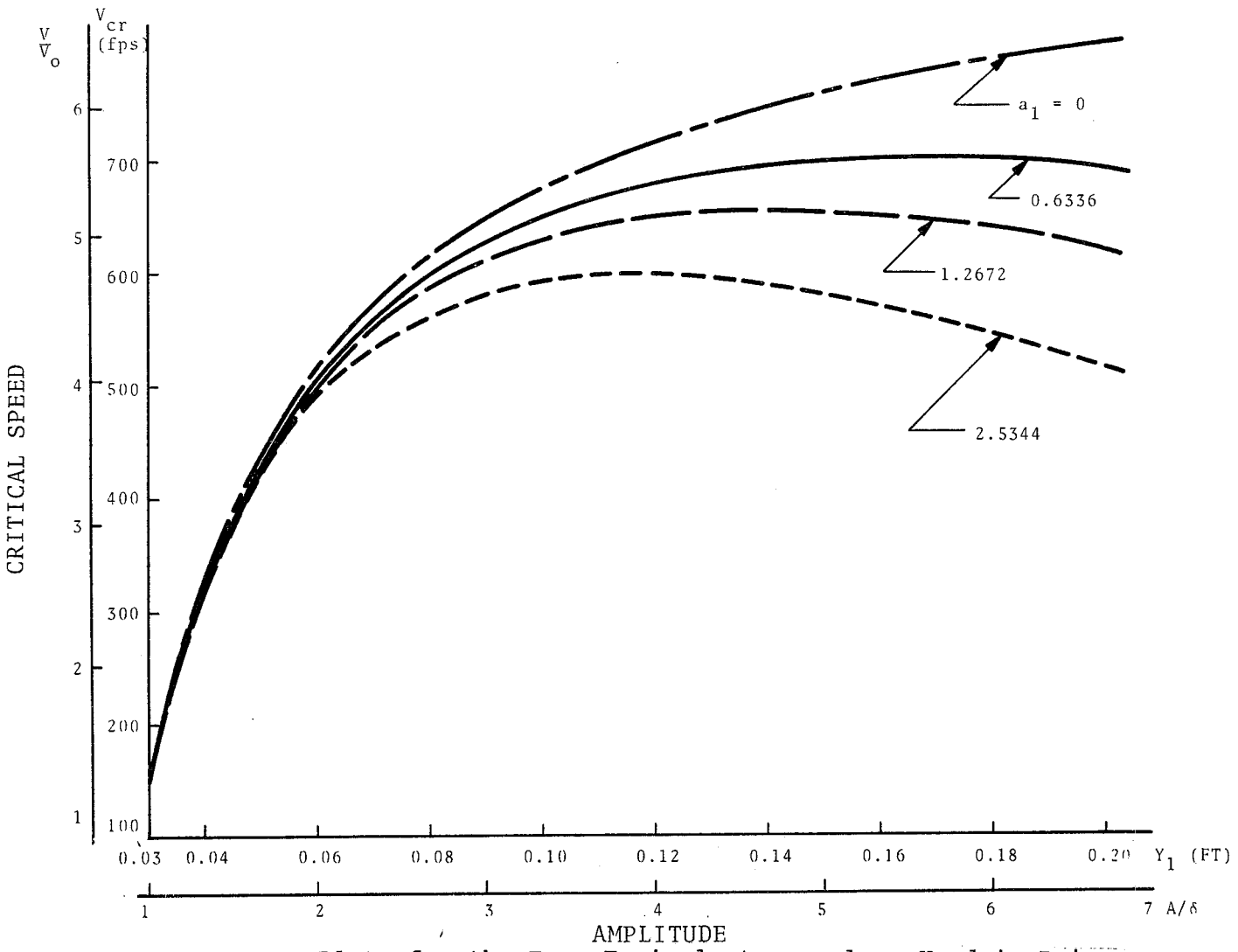

Figure B-1. Plots for the Four Equivalent a_1 Values Used in Prior Work. A Null Value of a_1 Corresponds to a Wheel with a Straight Conical Profile

The listing of computer program used to arrive at the results presented in Figure B-1 is shown in Figure B-2. The first part of the program includes the parameter values. Next, the describing function of gravitational stiffness in yaw and lateral directions and effective conicity are computed. The calculation of all the frequency parameters is carried out, and finally,the hunting frequency and critical speeds are evaluated.

```
      REAL KGS
      D0=0.0
      A0=0.0
      A1=0.05
      A2=0.0
      A3=2.53442
      A4=0.0
      A5=0.0
      R0=1.75
      AL=2.5
      AKY=10000.0
      AKS=105992.0
      AM=90.0
      C=360.0
      FT=3000000.0
      FL=FT
      W=AM*32.2
      WY=SQRT(AKY/AM)
      Y=0.005
      TYPE 5
5     FORMAT(9X,'Y',8X,'W(SI)',8X,'W(T)',8X,'W(L)',8X,'W(Y)',
     1 8X,'W(K)',//)
      TYPE 6
6     FORMAT(17X,'ALPHA(E)',4X,'BETA(E)',7X,'KA*',9X,'KG*',9X,'UCR'
     1 ,//)
      DO 100 I=1,20
      AKAS=W*AL*((A1+2.*A2*D0+3.*A3*D0**2+4.*A4*D0**3
     1 +5.*A5*D0**4)+.5*(3.*A3+12.*A4*D0+30.*A5*D0**2)
     2 *Y**2+.375*(5.*A5)*Y**4)
      COMP1=A1+2.*D0*A2+3.*D0**2*A3+4.*D0**3*A4+5.*D0**4*A5
      COMP2=A1-2.*D0*A2-4.*A2*D0-6.*A3*D0**2
      COMP3=9.*A3*D0**2-12.*A4*D0**3+16.*A4*D0**3-20.*A5*D0**4
      COMP4=25.*A5*D0**4+2.*A2*AL+6.*A3*D0*AL+12.*A4*D0**2*AL
      COMP5=20.*A5*D0**3*AL
      C1=COMP1+COMP2+COMP3+COMP4+COMP5
      COMPA=A3+4.*A4*D0+10.*A5*D0**2+3.*A3-4.*A4*D0
      COMPB=16.*A4*D0-20.*A5*D0**2+50.*A5*D0**2+4.*A4*AL
      COMPC=20.*A5*D0*AL
      C3=COMPA+COMPB+COMPC
      C5=6.*A5
      KGS=(C1+.75*C3*Y**2+.625*C5*Y**4)*W/AL
      ALPHAE=(A1+2.*A2*D0+3.*A3*D0**2+4.*A4*D0**3+5.*A5*D0**4)
     1 +.5*(A3+4.*A4*D0+10.*A5*D0**2)*Y**2+.375*A5*Y**4
      BETAE=SQRT((R0*AL)/(ALPHAE))
      WSE=SQRT((AKS-AKAS)/C)
      WT=SQRT((2.*FT*AL**2)/(C*BETAE))
      WL=SQRT((2.*FL)/(AM*BETAE))
      WGF2=KGS/AM
      WG2=WGF2+WY**2
      WG=SQRT(WG2)
      X=WSE**2+((WT/WL)**2)*WG**2
      R=WSE**4-2.*(WSE**2)*(WG**2)+WG**4
      S=1.+(WT**2/WL**2)
      T=WL**4+2.*(WT**2)*(WL**2)+WT**4
      Z=1.-R/T
      WKS=X/(S*Z)
      WK=SQRT(WKS)
      UCR=BETAE*WK
      TYPE 17,Y,WSE,WT,WL,WY,WK
17    FORMAT(6F12.4)
      TYPE 18,ALPHAE,BETAE,AKAS,KGS,UCR
18    FORMAT(13X,5F12.4,//)
100   Y=Y+.005
      STOP
      END
```

Figure B-2. Listing of Computer Program Using the Describing Function Technique for the Example of Prior Work

APPENDIX C

LISTING OF COMPUTER PROGRAM FOR IMPLEMENTING THE DESCRIBING FUNCTION TECHNIQUE

This Appendix includes a listing and typical output of the computer program developed to implement the describing function method presented in this report. The listing shown is for the case of a new wheel with a conical profile. Similar programs were used for the tread-worn conical and cylindrical profiles.

First, the coefficients of the least-square polynomial fit, as obtained from subprogram FITIT, are listed as A0, A1, ..., A18. Next, the coefficients used in the expressions for describing function are provided as C2, C4, ..., C20. The values of parameters are fed as RO for r_o, AL for ℓ, AKY for k_y, AKS for k_ψ, AM for m, FT for f_T and FL for f_L.

The expressions for describing function are computed, KGS for K_g^*, AKAS for K_a^* and ALPHAE for α_e^*. Using the computed value of α_e^*, β_e is calculated as BETAE. The values of equivalent frequencies from the expressions derived in Section 4 are computed as WSE for ω_{ψ_e}, WT for ω_T, WL for ω_L and WG for ω_g. The hunting frequency ω_k is calculated from the condition derived in Section 4, and the critical velocity V_{cr}, designated as VCR in the program, is calculated using ω_k and β_e.

For each value of oscillation amplitude Y, the steady-state value of yaw displacement ψ, creepage ξ_T and ξ_L, creep forces F_{C_T} and F_{C_L}, and gravitational force F_g are computed. The corresponding FORTRAN variable names are SI, CVT, CVL, CFT, CFL, and FG.

In the output, first the polynomial coefficients are listed. The computed values of various variables for each iteration of Y appear as three rows of output. These are illustrated by printing the FORTRAN variables following the values of polynomial coefficients. The equivalent variables used in dynamic equations are listed along with the FORTRAN variables. The plots in Section 6 are generated from the values thus computed for various tire profiles.

```
10      FORMAT(12X,'A0',15X,'A1',15X,'A2',15X,'A3',/)
        TYPE 12,A0,A1,A2,A3
        TYPE 14
14      FORMAT(12X,'A4',15X,'A5',15X,'A6',15X,'A7',/)
        TYPE 12,A4,A5,A6,A7
        TYPE 16
16      FORMAT(12X,'A8',15X,'A9',15X,'A10',14X,'A11',/)
        TYPE 12,A8,A9,A10,A11
1       TYPE 19
19      FORMAT(12X,'A12',14X,'A13',14X,'A14',14X,'A15',/)
        TYPE 12,A12,A13,A14,A15
        TYPE 20
20      FORMAT(12X,'A16',14X,'A17',14X,'A18',14X,'A19',/)
        TYPE 12,A16,A17,A18,A19
        TYPE 21
21      FORMAT(12X,'A20',14X,'A21',/)
        TYPE 13 ,A20,A21
12      FORMAT(4D17.6,//)
13      FORMAT(2D17.6,//)
        TYPE 5
5       FORMAT(///,9X,'Y',8X,'W(SI)',8X,'W(T)',8X,'W(L)',8X,'W(Y)',
     1  8X,'W(K)',//)
        TYPE 6
6       FORMAT(17X,'ALPHA(E)',4X,'BETA(E)',7X,'KA*',9X,'KG*',9X,'UCR'
     1  ,//)
        TYPE 50
50      FORMAT(9X,'SI',8X,'CUT',9X,'CFT',9X,'CUL',9X,'CFL',9X,
     1  'FG',//)
        DO 100 I=1,20
        KGS=W/AL*(2.*(A1+A2*AL)+4.*(A3+A4*AL)*(2.*C4)*Y**2+6.*(A5+A6*AL)
     1  *(2.*C6)*Y**4+8.*(A7+A8*AL)*(2.*C8)*Y**6+10.*(A9+A10*AL)*(2.*C10
     2  )*Y**8+12.*(A11+A12*AL)*(2.*C12)*Y**10+14.*(A13+A14*AL)*
     3  (2.*C14)*Y**12+16.*(A15+A16*AL)*(2.*C16)*Y**14+18.*(A17+A18*AL)*
     4  (2.*C18)*Y**16+20.*(A19+A20*AL)*(2.*C20)*Y**18+21*A21
     5  *(1.3749309/4.0874803)*Y**20)
        ALPHAE=A1+A3*C2*Y**2+A5*C4*Y**4+A7*C6*Y**6+A9*C8*Y**8+A11
     1  *C10*Y**10+A13*C12*Y**12+A15*C14*Y**14+A17*C16*Y**16+A19
     2  *C18*Y**18+A21*C20*Y**20
        AKAS=W*AL*(A1+3.*A3*C2*Y**2+5.*A5*C4*Y**4+7.*A7*C6*Y**6
     1  +9.*A9*C8*Y**8+11.*A11*C10*Y**10+13.*A13*C12*Y**12+15.*A15
     2  *C14*Y**14+17.*A17*C16*Y**16+19.*A19*C18*Y**18+21.*A21*C20
     3  *Y**20)
        AGS=KGS*1.0E06/(KGS+1.0E06)
        KGS=AGS
        BETAE=SQRT((R0*AL)/(ALPHAE))
        WSE=SQRT((AKS-AKAS)/C)
        WT=SQRT((2.*FT*AL**2)/(C*BETAE))
        WL=SQRT((2.*FL)/(AM*BETAE))
```

```
      WGF2=KGS/AM
      WG2=WGF2+WY**2
      WG=SQRT(WG2)
      X=WSE**2+((WT/WL)**2)*WG**2
      R=WSE**4-2.*(WSE**2)*(WG**2)+WG**4
      S=1.+(WT**2/WL**2)
      T=WL**4+2.*(WT**2)*(WL**2)+WT**4
      Z=1.-R/T
      WKS=X/(S*Z)
      WK=SQRT(WKS)
      VCR=BETAE*WK
      SI=(SQRT(((KGS+AKY)-(AM*WK**2))**2+(2.*FL/BETAE)**2)
     1 /(2.*FL))*Y
      CVT=SQRT((ALPHAE*Y/R0)**2+(SI*AL/BETAE)**2)
      CFT=FT*CVT
      CVL=SQRT((Y/BETAE)**2+SI**2)
      CFL=FL*CVL
      FG=(2.*W/AL)*((A1+A2*AL)*Y+2.*(A3+A4*AL)*Y**3+3.*(A5+A6*AL)*Y**5
     1 +4.*(A7+A8*AL)*Y**7+5.*(A9+A10*AL)*Y**9+6.*(A11+A12*AL)
     2 *Y**11+7.*(A13+A14*AL)*Y**13+8.*(A15+A16*AL)*Y**15
     3 +9.*(A17+A18*AL)*Y**17+10.*(A19+A20*AL)*Y**19)
      TYPE 17,Y,WSE,WT,WL,WY,WK
17    FORMAT(6F12.4)
      TYPE 18,ALPHAE,BETAE,AKAS,KGS,VCR
18    FORMAT(13X,5F12.4)
      TYPE 55,SI,CVT,CFT,CVL,CFL,FG
55    FORMAT(6E12.4,///)
100   Y=Y+.01
      STOP
      END
```

```
.EX RICNU.F4
FORTRAN:  RICNU.F4
LOADING

RICNU 3K CORE
EXECUTION
```

A0	A1	A2	A3
0.157856D-04	0.515547D-01	-0.363341D-01	-0.496025D+00
A4	**A5**	**A6**	**A7**
0.190724D+02	-0.378107D+03	-0.337622D+04	0.175136D+06
A8	**A9**	**A10**	**A11**
-0.346927D+05	-0.321234D+08	0.397835D+08	0.325194D+10
A12	**A13**	**A14**	**A15**
0.985634D+09	-0.159872D+12	-0.248103D+12	0.367508D+13
A16	**A17**	**A18**	**A19**
0.874195D+13	-0.319845D+14	-0.941451D+14	0.000000D+00
A20	**A21**		
0.000000D+00	0.000000D+00		

Y(γ)	W(SI) ω_ψ	W(T) ω_T	W(L) ω_L	W(Y) ω_{y_0}	W(K) ω_{k_0}
	ALPHA(E) α_E^*	BETA(E) β_{E_0}	KA* $K_{a_0}^*$	KG* K_γ^*	VCR V_{cr}
SI ψ	CUT E_T	CFT F_{c_T}	CUL E_L	CFL F_{c_L}	FG F_γ

```
FLOATING UNDERFLOW       PC=000776

FLOATING UNDERFLOW       PC=001015

     0.0050      16.6355      40.3534      32.2827      23.5702      21.2378
                  0.0515       8.5292     373.3757     -86.9975     181.1411
 0.5891E-03  0.2436E-03  0.9744E+02  0.8311E-03  0.3324E+03 -0.4282E+00


     0.0150      16.6356      40.3424      32.2739      23.5702      21.2432
                  0.0515       8.5338     372.0709     -56.0855     181.2860
 0.1766E-02  0.7300E-03  0.2920E+03  0.2492E-02  0.9968E+03 -0.6740E+00


     0.0250      16.6359      40.3157      32.2526      23.5702      21.2526
                  0.0514       8.5451     368.7343      -3.3148     181.6060
 0.2940E-02  0.1213E-02  0.4854E+03  0.4148E-02  0.1659E+04  0.5510E+00


     0.0350      16.6364      40.2695      32.2156      23.5702      21.2631
                  0.0511       8.5648     363.1799      54.1851     182.1133
 0.4107E-02  0.1691E-02  0.6765E+03  0.5794E-02  0.2317E+04  0.3092E+01


     0.0450      16.6369      40.2066      32.1653      23.5702      21.2709
                  0.0508       8.5916     356.9019      95.0743     182.7506
 0.5264E-02  0.2161E-02  0.8643E+03  0.7426E-02  0.2970E+04  0.5503E+01


     0.0550      16.6372      40.1393      32.1114      23.5702      21.2734
                  0.0505       8.6204     352.8203     104.5269     183.3858
 0.6413E-02  0.2623E-02  0.1049E+04  0.9046E-02  0.3618E+04  0.5998E+01


     0.0650      16.6371      40.0858      32.0686      23.5702      21.2727
                  0.0502       8.6434     354.3594      96.5221     183.8692
 0.7559E-02  0.3084E-02  0.1234E+04  0.1066E-01  0.4265E+04  0.6164E+01


     0.0750      16.6361      40.0700      32.0560      23.5702      21.2814
                  0.0501       8.6503     366.9804     148.4584     184.0901
 0.8715E-02  0.3553E-02  0.1421E+04  0.1229E-01  0.4917E+04  0.1888E+02
```

0.0850	16.6329	40.1343	32.1074	23.5702	21.3289
	0.0504	8.6226	405.3098	436.7002	183.9103
0.9909E-02	0.4053E-02	0.1621E+04	0.1398E-01	0.5591E+04	0.7937E+02
0.0950	16.6246	40.3696	32.2957	23.5702	21.4606
	0.0516	8.5223	504.2735	1241.8632	182.8937
0.1121E-01	0.4637E-02	0.1855E+04	0.1581E-01	0.6323E+04	0.2519E+03
0.1050	16.6063	40.9405	32.7524	23.5702	21.7238
	0.0546	8.2863	723.6387	2875.5813	180.0099
0.1274E-01	0.5422E-02	0.2169E+04	0.1797E-01	0.7189E+04	0.6163E+03
0.1150	16.5724	42.0481	33.6385	23.5702	22.1347
	0.0608	7.8555	1127.8236	5490.5990	173.8794
0.1473E-01	0.6609E-02	0.2644E+04	0.2077E-01	0.8307E+04	0.1215E+04
0.1250	16.5220	43.7961	35.0369	23.5702	22.6369
	0.0715	7.2410	1728.1195	8804.6534	163.9126
0.1738E-01	0.8457E-02	0.3383E+04	0.2449E-01	0.9798E+04	0.1958E+04
0.1350	16.4650	46.0452	36.8362	23.5702	23.0835
	0.0874	6.5509	2405.1434	11903.7170	151.2170
0.2074E-01	0.1116E-01	0.4463E+04	0.2924E-01	0.1170E+05	0.2547E+04
0.1450	16.4244	48.4169	38.7335	23.5702	23.2803
	0.1068	5.9248	2886.2064	13432.4578	137.9310
0.2462E-01	0.1465E-01	0.5859E+04	0.3471E-01	0.1388E+05	0.2544E+04
0.1550	16.4235	50.4648	40.3718	23.5702	23.1093
	0.1261	5.4537	2897.2691	12473.9276	126.0311
0.2856E-01	0.1847E-01	0.7388E+04	0.4029E-01	0.1612E+05	0.1771E+04

```
     0.1650      16.4555      51.9144      41.5315      23.5702      22.7080
                  0.1412       5.1534    2517.9300    9905.6731     117.0228
 0.3214E-01  0.2201E-01  0.8803E+04  0.4537E-01  0.1815E+05  0.8787E+03


     0.1750      16.4778      52.8601      42.2881      23.5702      22.4041
                  0.1518       4.9706    2253.6501    7958.2968     111.3626
 0.3532E-01  0.2508E-01  0.1003E+05  0.4987E-01  0.1995E+05  0.5992E+03


     0.1850      16.5968      53.3507      42.6806      23.5702      21.1547
                  0.1575       4.8796     836.8768     -48.9981     103.2271
 0.3798E-01  0.2749E-01  0.1100E+05  0.5366E-01  0.2147E+05 -0.5645E+04


ATTEMPT TO TAKE SQRT OF NEGATIVE ARG     PC=001404

     0.1950      17.8521      49.5915      39.6732      23.5702      17.2823
                  0.1176       5.6475 -14731.3580 -75724.7383      97.6010
 0.3683E-01  0.2235E-01  0.8940E+04  0.5049E-01  0.2019E+05 -0.6009E+05


CPU TIME: 3.47  ELAPSED TIME: 4:29.45

NO. OF ERRORS           ERROR TYPE
8               FLOATING UNDERFLOW
1               ATTEMPT TO TAKE SQRT OF NEGATIVE ARG

EXIT
```